Second-order quantum corrections for the frustrated spatially anisotropic spin-$\frac{1}{2}$ Heisenberg antiferromagnet on a square lattice

Kingshuk Majumdar*
Department of Physics, Grand Valley State University, Allendale, Michigan 49401, USA
(Received 3 July 2010; revised manuscript received 5 August 2010; published 4 October 2010)

The effects of quantum fluctuations due to directional anisotropy and frustration between nearest neighbors and next-nearest neighbors of the quantum spin-$\frac{1}{2}$ Heisenberg antiferromagnet on a square lattice are investigated using spin-wave expansion. We have calculated the spin-wave-energy dispersion in the entire Brillouin zone, renormalized spin-wave velocities, and the magnetization up to second order in $1/S$ expansion for the antiferromagnetic Neél and collinear antiferromagnetic stripe phases. It is shown that the second-order corrections become significant with increase in frustration. With these corrections magnetizations and spin-wave velocities for both the phases become zero at the quantum critical points as expected from other numerical and analytical methods. We have shown that the transition between the two ordered phases are always separated by the disordered paramagnetic phase.

DOI: 10.1103/PhysRevB.82.144407 PACS number(s): 75.10.Jm, 75.40.Mg, 75.50.Ee, 73.43.Nq

I. INTRODUCTION

The physics of two-dimensional (2D) frustrated spin-$\frac{1}{2}$ Heisenberg antiferromagnet continues to attract considerable attention due to the discovery and availability of new magnetic materials such as the layered oxide high-temperature superconductors.[1–11] These systems can be well described by the Heisenberg spin model with nearest-neighbor (NN) antiferromagnetic coupling J_1 and next-nearest-neighbor (NNN) antiferromagnetic coupling J_2. Experimentally by applying high pressures the ground state phase diagram of these frustrated spin systems can be explored from low $\eta=J_2/J_1$ to high η. For example, Li_2VOSiO_4 is an insulating vanadium oxide, with spin $s=1/2$ V^{4+} ions arranged in square lattice planes at the centers of VO_4 pyramids. These are linked by SiO_4 tetrahedra with Li ions occupying the space between the V-O planes. X-ray diffraction measurements on this compound show that the value of η decreases by about 40% with increase in pressure from zero to 7.6 GPa.[12] Moreover, nuclear magnetic resonance, magnetization, specific heat, and muon spin-rotation measurements on these compounds [Li_2VOSiO_4, Li_2VOGeO_4, $VOMoO_4$, and $BaCdVO(PO_4)_2$] show significant coupling between NN and NNN neighbors.[4–6] In addition these experiments on Li_2VOSiO_4 have shown that it undergoes a phase transition at a low temperature (2.8 K) to collinear antiferromagnetic order with magnetic moments lying in the a-b plane with $J_2+J_1 \sim 8.2(1)$ K and $J_2/J_1 \sim 1.1(1)$.[6,7]

Quantum spin-$\frac{1}{2}$ antiferromagnetic J_1-J_2 model on a square lattice has been studied extensively by various analytical and numerical techniques such as the diagrammatic perturbation theory based on spin-wave expansion,[13–24] modified spin-wave theory,[25] field theory,[26–32] series expansion,[33–38] exact diagonalization,[39] density matrix renormalization group (DMRG),[40–42] effective field theory,[43,44] coupled cluster method,[45] band-structure calculations,[46] and Quantum Monte Carlo.[47–49] It is now well known that at low temperatures these systems exhibit new types of magnetic order and novel quantum phases.[50,51] For $J_2=0$ the ground state is antiferromagnetically ordered at zero temperature. Addition of next-nearest-neighbor interactions induces a strong frustration and break the antiferromagnetic (AF) order at $J_2 \sim J_1/2$. The competition between NN and NNN interactions for the square lattice is characterized by the frustration parameter $\eta=J_2/J_1$. It has been found that a disordered paramagnetic phase exists between $\eta_{1c} \approx 0.38$ and $\eta_{2c} \approx 0.60$.[52,53] For $\eta < \eta_{1c}$ the square lattice is AF ordered whereas for $\eta > \eta_{2c}$ a degenerate collinear antiferromagnetic (CAF) stripe phase emerges. In the collinear state the NN spins have a parallel orientation in the vertical direction and antiparallel orientation in the horizontal direction or vice versa. The exact nature of the phase transitions and the nature of the intermediate phase are still debatable. It is believed that the phase transition from the AF-ordered state to the intermediate paramagnetic state at η_{1c} is of second order and from the paramagnetic state to the collinear state at η_{2c} is of first order.[52,53]

A generalization of the frustrated J_1-J_2 model is the J_1-J_1'-J_2 model where $\zeta=J_1'/J_1$ is the directional anisotropy parameter.[28,31] It is known that the spatial anisotropy reduces the width of the disordered phase. Extensive band structure calculations[46] for the vanadium phosphate compounds $Pb_2VO(PO_4)_2$, $SrZnVO(PO_4)_2$, $BaZnVO(PO_4)_2$, and $BaCdVO(PO_4)_2$ have shown four different exchange couplings: J_1 and J_1' between the NN and J_2 and J_2' between NNN. For example $\zeta \approx 0.7$ and $J_2'/J_2 \approx 0.4$ were obtained for $SrZnVO(PO_4)_2$. A possible realization of the J_1-J_1'-J_2 model may be the compound $(NO)Cu(NO_3)_3$ (Ref. 54) though recent band-structure calculations show a uniform spin chain model with different types of anisotropy and weak interchain couplings.[55] Within the spin-wave expansion the effect of directional anisotropy on the spin-wave-energy dispersion and the transverse dynamical structure factor has been studied before.[15] However, the effect of NNN frustration has not been incorporated in that study.

For the J_1-J_1'-J_2 model using a higher order coupled cluster method Bishop *et al.*[45] reported existence of a quantum triple point (QTP) at $\zeta \approx 0.60$, $\eta \approx 0.33$. Below this point they predicted a second-order phase transition between the quantum Neél and stripe phases whereas above it these two

phases are separated by an intermediate phase. Existence of a QTP has also been reported by other authors[43,44] where they used effective field theory and effective renormalization group approach to obtain a QTP at $\zeta=0.51$, $\eta\approx 0.28$. In a DMRG study it was predicted that there is no intermediate phase (no spin gap) for η lower than 0.287 when $\zeta=1$ (isotropic case).[40] But more recent DMRG calculations have concluded that a disordered paramagnetic region persists for all $\eta>0$.[41]

It should be mentioned that the present J_1-J_1'-J_2 model was introduced[31] as a 2D generalization of the frustrated two-leg ladder. However, the phases of the frustrated J_1-J_1'-J_2 Heisenberg model differs from the phase diagram of the frustrated spin-$\frac{1}{2}$ ladder with rung coupling J_1' and diagonal coupling J_2.[56,57] In case of the frustrated spin-$\frac{1}{2}$ ladder for $J_1'<2J_2$ the ground state is of Haldane type, with two spin-$\frac{1}{2}$ on the rung forming effective spin-1. On the other hand for $J_1'>2J_2$ rung pairs form singlets, resulting in the rung-singlet phase.[28]

Frustrated two leg ladders share some common features with the present 2D J_1-J_1'-J_2 model. Using bosonization calculations it has been shown that a spin gap and dimerization are also present in this case.[28] However, the presence of this intermediate phase has been questioned and a direct transition from the rung singlet to the Haldane phase has been reported.[58,59] Yet evidence of such a dimerized intermediate phase in the two leg model was found numerically in Refs. 56 and 57 up to a certain value of the interchain coupling.

One of the main motivations of this work is to investigate (within second-order spin-wave expansion) if a disordered paramagnetic region exists for this frustrated, spatially anisotropic J_1-J_1'-J_2 model on a square lattice. We find that the intermediate disordered phase exist even for small spatial anisotropies.

In this work we present a comprehensive study of the effect of zero-temperature quantum fluctuations on the spin wave energy, spin-wave velocities, and magnetization for the two ordered phases of the J_1-J_1'-J_2 Heisenberg AF on a square lattice. We use spin-wave expansion based on Holstein-Primakoff transformation up to second order to numerically calculate the physical quantities. Whenever possible we compare our results with available experimental data on the systems mentioned above and with other existing analytical or numerical results. The paper is organized as follows. Section II provides an introduction to the Hamiltonian for the Heisenberg spin-$\frac{1}{2}$ AF on a spatially anisotropic square lattice. The classical ground-state configurations of the model and the different phases are then briefly discussed. In the next two sections Secs. II A and II B the spin Hamiltonian is mapped to the Hamiltonian of interacting spin-wave excitations (magnons) and spin-wave expansion up to second order for spin-wave energy, spin-wave velocities, and staggered magnetizations are presented for the two ordered phases. These physical quantities for the two phases are numerically calculated and the results are plotted and discussed in Sec. III. Finally we summarize our results in Sec. IV. Appendices A–C contain details of the formalism.

II. MODEL

We consider a frustrated $S=\frac{1}{2}$ antiferromagnet with spatial anisotropy on a $N_L\times N_L$ square lattice with three types of exchange interactions between spins: J_1 along the x (row) directions, J_1' along the y (column) directions, and J_2 along the diagonals. We assume all interactions to be antiferromagnetic and positive, i.e., $J_1,J_1',J_2>0$. This J_1-J_1'-J_2 spin system is described by the Heisenberg Hamiltonian

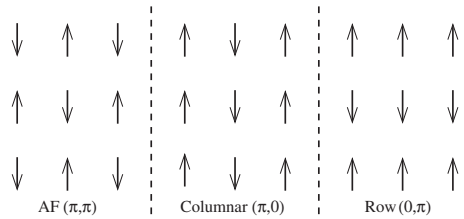

FIG. 1. Classical ground states: (a) AF (π,π), (b) columnar $(\pi,0)$, and (c) row $(0,\pi)$.

$$H=\frac{1}{2}J_1\sum_{i=1}^{N}\mathbf{S}_i\cdot\mathbf{S}_{i+\delta_x}+\frac{1}{2}J_1'\sum_{i=1}^{N}\mathbf{S}_i\cdot\mathbf{S}_{i+\delta_y}+\frac{1}{2}J_2\sum_{i=1}^{N}\mathbf{S}_i\cdot\mathbf{S}_{i+\delta_x+\delta_y}, \tag{1}$$

where i runs over all lattice sites and $i+\delta_x$ ($\delta_x=\pm 1$) and $i+\delta_y$ ($\delta_y=\pm 1$) are the nearest neighbors to the ith site along the row and the column direction. The third term represents the interaction between the next-nearest neighbors, which are along the diagonals.

At zero temperature this model exhibits three types of classical ground-state configurations: the Neél state or the (π,π) state and the two stripe states which are the columnar stripe $(\pi,0)$ and the row stripe $(0,\pi)$. The spin orientations of these three states are shown in Fig. 1. The Neél state breaks the SU(2) and the lattice translational symmetry but preserves the fourfold rotational symmetry C_4 of the square. The stripe states break SU(2) and partial lattice translational symmetries (along one direction). In addition this state breaks the invariance under $\pi/2$ real-space rotations C_4 to C_2.

The classical ground-state energies of these states are determined by treating the spins as classical vectors and then minimizing the energy. These are

$$E_{\mathrm{AF}}^{cl}/N=-\frac{1}{2}J_1S^2z[1+\zeta-2\eta],$$

$$E_{\mathrm{columnar}}^{cl}/N=-\frac{1}{2}J_1S^2z[1-\zeta+2\eta],$$

$$E_{\mathrm{row}}^{cl}/N=-\frac{1}{2}J_1S^2z[-1+\zeta+2\eta]. \tag{2}$$

Here $\zeta=J_1'/J_1$ is the directional anisotropy parameter and $\eta=J_2/J_1$ is the magnetic frustration between the NN (row direction) and NNN spins. $z=2$ is the number of nearest neighbor sites. Equation (2) shows that the classical ground state is either the AF Neél state for $\eta<\zeta/2$ or the CAF stripe state if $\eta>\zeta/2$. The classical first-order phase transition between the AF and CAF state occurs at the critical value $\eta_c^{\mathrm{class}}=\zeta/2$.[45]

At low temperature quantum fluctuations play a significant role on the phase diagram of the system. In the next sections we will consider the classical spins as quantum spins and study the role of quantum fluctuations on the AF and CAF ordered phases. We follow a standard procedure by first expressing the fluctuations around the "classical" ground state in terms of the boson operators using the Holstein-Primakoff transformation.[60] The quadratic term in boson operators corresponds to the linear spin-wave theory whereas the higher order terms represent spin-wave (magnon) interactions. We keep terms up to second order in $1/S$. In the next step we calculate the renormalized magnon Green's functions and self-energies. Finally, we calculate the magnon energy dispersion, renormalized spin-wave velocities, and the staggered magnetization per spin to the leading order in $1/S^2$ for the AF and CAF phases.

A. AF phase: Formalism

For the AF ordered phase NN interactions are between A and B sublattices and NNN interactions are between A-A and B-B sublattices. The Hamiltonian in Eq. (1) takes the form

$$H = J_1 \sum_i \mathbf{S}_i^{\mathrm{A}} \cdot \mathbf{S}_{i+\delta_x}^{\mathrm{B}} + J_1' \sum_i \mathbf{S}_i^{\mathrm{A}} \cdot \mathbf{S}_{i+\delta_y}^{\mathrm{B}} + \frac{1}{2} J_2 \sum_i [\mathbf{S}_i^{\mathrm{A}} \cdot \mathbf{S}_{i+\delta_x+\delta_y}^{\mathrm{A}} + \mathbf{S}_i^{\mathrm{B}} \cdot \mathbf{S}_{i+\delta_x+\delta_y}^{\mathrm{B}}]. \tag{3}$$

This Hamiltonian can be mapped into an equivalent Hamiltonian of interacting bosons by transforming the spin operators to bosonic creation and annihilation operators $a^\dagger, a$ for "up" and $b^\dagger, b$ for "down" sublattices using the Holstein-Primakoff transformations keeping only terms up to the order of $1/S^2$

$$S_{Ai}^+ \approx \sqrt{2S}\left[1 - \frac{1}{2}\frac{a_i^\dagger a_i}{(2S)} - \frac{1}{8}\frac{a_i^\dagger a_i a_i^\dagger a_i}{(2S)^2}\right] a_i,$$

$$S_{Ai}^- \approx \sqrt{2S} a_i^\dagger \left[1 - \frac{1}{2}\frac{a_i^\dagger a_i}{(2S)} - \frac{1}{8}\frac{a_i^\dagger a_i a_i^\dagger a_i}{(2S)^2}\right],$$

$$S_{Ai}^z = S - a_i^\dagger a_i,$$

$$S_{Bj}^+ \approx \sqrt{2S} b_j^\dagger \left[1 - \frac{1}{2}\frac{b_j^\dagger b_j}{(2S)} - \frac{1}{8}\frac{b_j^\dagger b_j b_j^\dagger b_j}{(2S)^2}\right],$$

$$S_{Bj}^- \approx \sqrt{2S}\left[1 - \frac{1}{2}\frac{b_j^\dagger b_j}{(2S)} - \frac{1}{8}\frac{b_j^\dagger b_j b_j^\dagger b_j}{(2S)^2}\right] b_j,$$

$$S_{Bj}^z = -S + b_j^\dagger b_j. \tag{4}$$

Substituting Eq. (4) we expand the Hamiltonian in powers of $1/S$ as

$$H = -\frac{1}{2} N J_1 S^2 z(1+\zeta)\left[1 - \frac{2\eta}{1+\zeta}\right] + H_0 + H_1 + H_2 + \cdots. \tag{5}$$

The first term corresponds to the classical energy of the AF ground state [Eq. (2)]. Next using the spatial Fourier transforms

$$a_i = \sqrt{\frac{2}{N}} \sum_{\mathbf{k}} e^{-i\mathbf{k}\cdot\mathbf{R_i}} a_{\mathbf{k}}, \quad b_j = \sqrt{\frac{2}{N}} \sum_{\mathbf{k}} e^{-i\mathbf{k}\cdot\mathbf{R_j}} b_{\mathbf{k}}$$

the real space Hamiltonian is transformed to the $\mathbf{k}$-space Hamiltonian. Momentum $\mathbf{k}$ is defined in the first Brillouin zone (BZ): $-\pi < k_x \leq \pi$, $-\pi < k_y \leq \pi$ (with unit lattice spacing). The reduced Brillouin zone contains $N/2$ $\mathbf{k}$ vectors as the unit cell is a magnetic supercell consisting of an A site and a B site.

Furthermore, we diagonalize the quadratic part H_0 by transforming the operators $a_{\mathbf{k}}$ and $b_{\mathbf{k}}$ to magnon operators $\alpha_{\mathbf{k}}$ and $\beta_{\mathbf{k}}$ using the Bogoliubov (BG) transformations

$$a_{\mathbf{k}}^\dagger = l_{\mathbf{k}} \alpha_{\mathbf{k}}^\dagger + m_{\mathbf{k}} \beta_{-\mathbf{k}}, \quad b_{-\mathbf{k}} = m_{\mathbf{k}} \alpha_{\mathbf{k}}^\dagger + l_{\mathbf{k}} \beta_{-\mathbf{k}}, \tag{6}$$

where the coefficients $l_{\mathbf{k}}$ and $m_{\mathbf{k}}$ are defined as

$$l_{\mathbf{k}} = \left[\frac{1+\epsilon_{\mathbf{k}}}{2\epsilon_{\mathbf{k}}}\right]^{1/2}, \quad m_{\mathbf{k}} = -\,\mathrm{sgn}(\gamma_{\mathbf{k}}) \left[\frac{1-\epsilon_{\mathbf{k}}}{2\epsilon_{\mathbf{k}}}\right]^{1/2} \equiv -x_{\mathbf{k}} l_{\mathbf{k}} \tag{7}$$

with

$$\epsilon_{\mathbf{k}} = (1 - \gamma_{\mathbf{k}}^2)^{1/2},$$

$$\gamma_{\mathbf{k}} = \gamma_{1\mathbf{k}}/\kappa_{\mathbf{k}},$$

$$\gamma_{1\mathbf{k}} = [\cos(k_x) + \zeta \cos(k_y)]/(1+\zeta),$$

$$\gamma_{2\mathbf{k}} = \cos(k_x)\cos(k_y),$$

$$\kappa_{\mathbf{k}} = 1 - \frac{2\eta}{1+\zeta}(1 - \gamma_{2\mathbf{k}}). \tag{8}$$

$\gamma_{\mathbf{k}}$ is negative in certain parts of the first BZ—so it is essential to keep track of the sign of $\gamma_{\mathbf{k}}$ through the function $\mathrm{sgn}(\gamma_{\mathbf{k}})$. After these transformations, the quadratic part of the Hamiltonian becomes

$$H_0 = J_1 S z (1+\zeta) \sum_{\mathbf{k}} \kappa_{\mathbf{k}} (\epsilon_{\mathbf{k}} - 1) + J_1 S z (1+\zeta) \sum_{\mathbf{k}} \kappa_{\mathbf{k}} \epsilon_{\mathbf{k}} (\alpha_{\mathbf{k}}^\dagger \alpha_{\mathbf{k}} + \beta_{\mathbf{k}}^\dagger \beta_{\mathbf{k}}). \tag{9}$$

The first term is the zero-point energy and the second term represents the excitation energy of the magnons within linear spin-wave theory (LSWT).

The part H_1 corresponds to $1/S$ correction to the Hamiltonian. We follow the same procedure as described above. The resulting expression after transforming the bosonic operators to the magnon operators is

$$H_1 = \frac{J_1 Sz(1+\zeta)}{2S}\sum_{\mathbf{k}}[A_{\mathbf{k}}(\alpha_{\mathbf{k}}^\dagger\alpha_{\mathbf{k}} + \beta_{\mathbf{k}}^\dagger\beta_{\mathbf{k}}) + B_{\mathbf{k}}(\alpha_{\mathbf{k}}^\dagger\beta_{-\mathbf{k}} + \beta_{-\mathbf{k}}\alpha_{\mathbf{k}})] - \frac{J_1 Sz(1+\zeta)}{2SN}\sum_{1234}\delta_{\mathbf{G}}(1+2-3-4)l_1 l_2 l_3 l_4[\alpha_1^\dagger\alpha_2^\dagger\alpha_3\alpha_4 V_{1234}^{(1)}$$
$$+ \beta_{-3}^\dagger\beta_{-4}^\dagger\beta_{-1}\beta_{-2}V_{1234}^{(2)} + 4\alpha_1^\dagger\beta_{-4}^\dagger\beta_{-2}\alpha_3 V_{1234}^{(3)} + \{2\alpha_1^\dagger\beta_{-2}\alpha_3\alpha_4 V_{1234}^{(4)} + 2\beta_{-4}^\dagger\beta_{-1}\beta_{-2}\alpha_3 V_{1234}^{(5)} + \alpha_1^\dagger\alpha_2^\dagger\beta_{-3}^\dagger\beta_{-4}^\dagger V_{1234}^{(6)} + \text{H.c.}\}]. \tag{10}$$

In the above equation momenta $\mathbf{k}_1, \mathbf{k}_2, \mathbf{k}_3, \mathbf{k}_4$ are abbreviated as 1, 2, 3, and 4. The first term in Eq. (10), which is known as the Oguchi correction[61] in the literature is obtained by setting the products of four boson operators into normal ordered forms with respect to the magnon operators, where $A_{\mathbf{k}}$ and $B_{\mathbf{k}}$ are

$$A_{\mathbf{k}} = A_1\frac{1}{\kappa_{\mathbf{k}}\epsilon_{\mathbf{k}}}[\kappa_{\mathbf{k}} - \gamma_{1\mathbf{k}}^2] + A_2\frac{1}{\epsilon_{\mathbf{k}}}[1-\gamma_{2\mathbf{k}}], \tag{11}$$

$$B_{\mathbf{k}} = B_1\frac{1}{\kappa_{\mathbf{k}}\epsilon_{\mathbf{k}}}\gamma_{1\mathbf{k}}[1-\gamma_{2\mathbf{k}}] \tag{12}$$

with

$$A_1 = \frac{2}{N}\sum_{\mathbf{p}}\frac{1}{\epsilon_{\mathbf{p}}}\left[\frac{\gamma_{1\mathbf{p}}^2}{\kappa_{\mathbf{p}}} + \epsilon_{\mathbf{p}} - 1\right], \tag{13}$$

$$A_2 = \left(\frac{2\eta}{1+\zeta}\right)\frac{2}{N}\sum_{\mathbf{p}}\frac{1}{\epsilon_{\mathbf{p}}}[1-\epsilon_{\mathbf{p}} - \gamma_{2\mathbf{p}}], \tag{14}$$

$$B_1 = \left(\frac{2\eta}{1+\zeta}\right)\frac{2}{N}\sum_{\mathbf{p}}\frac{1}{\epsilon_{\mathbf{p}}}\left[\gamma_{2\mathbf{p}} - \frac{\gamma_{1\mathbf{p}}^2}{\kappa_{\mathbf{p}}}\right]. \tag{15}$$

The second term in Eq. (10) represents scattering between spin waves, where the delta function $\delta_{\mathbf{G}}(1+2-3-4)$ ensures that momentum is conserved within a reciprocal lattice vector $\mathbf{G}$. Explicit forms of the vertex factors $V_{1234}^{i=1,\ldots,6}$ are given in Appendix A.

The second-order term, H_2 is composed of six boson operators. Before the BG transformation H_2 is of the following form:

$$H_2 = \frac{J_1 Sz(1+\zeta)}{(2S)^2N^2}\sum_{123456}\delta_{\mathbf{G}}(1+2+3-4-5-6)\Bigg(\gamma_1(2+3-6)a_1^\dagger a_4 a_5 b_{-6}^\dagger b_{-2}b_{-3} + \gamma_1(3-5-6)a_1^\dagger a_2^\dagger a_4 b_{-5}^\dagger b_{-6}^\dagger b_{-3}$$
$$-\frac{1}{2}[\gamma_1(4)a_4 b_{-5}^\dagger b_{-1}b_{-6}^\dagger b_{-2}b_{-3} + \gamma_1(3)a_1^\dagger a_4 a_2^\dagger a_5 a_6 b_{-3} + \text{H.c.}] + \left(\frac{2\eta}{1+\zeta}\right)\Bigg\{\gamma_2(2+3-6)a_1^\dagger a_4 a_5 a_2^\dagger a_3^\dagger a_6$$
$$+\gamma_2(3-5-6)a_1^\dagger a_2^\dagger a_4 a_3^\dagger a_5 a_6 - \frac{1}{2}[\gamma_2(3)a_1^\dagger a_4 a_2^\dagger a_5 a_6 a_3^\dagger + \gamma_2(1)a_1^\dagger a_2^\dagger a_4 a_3^\dagger a_5 a_6 + \text{H.c.}] + a\leftrightarrow b\Bigg\}\Bigg). \tag{16}$$

After transformation to magnon operators $\alpha_{\mathbf{k}}, \beta_{\mathbf{k}}$ the Hamiltonian in normal ordered form reduces to

$$H_2 = \frac{J_1 Sz(1+\zeta)}{(2S)^2}\sum_{\mathbf{k}}[C_{1\mathbf{k}}(\alpha_{\mathbf{k}}^\dagger\alpha_{\mathbf{k}} + \beta_{\mathbf{k}}^\dagger\beta_{\mathbf{k}}) + C_{2\mathbf{k}}(\alpha_{\mathbf{k}}^\dagger\beta_{-\mathbf{k}}^\dagger + \beta_{-\mathbf{k}}\alpha_{\mathbf{k}}) + \cdots]. \tag{17}$$

The dotted terms contribute to higher than second order corrections and are thus omitted in our calculations. The coefficients $C_{1\mathbf{k}}$ and $C_{2\mathbf{k}}$ are given in Appendix B. We will find that these corrections play a significant role in the magnon energy dispersion and in the phase diagram for large frustration and/or small anisotropy.

The quasiparticle energy $\tilde{E}_{\mathbf{k}}^{\text{AF}}$ for magnon excitations, measured in units of $J_1 Sz(1+\zeta)$ up to second order in $1/S$ is given as

$$\tilde{E}_{\mathbf{k}}^{\text{AF}} = E_{\mathbf{k}} + \frac{1}{(2S)}A_{\mathbf{k}} + \frac{1}{(2S)^2}\left[\Sigma_{\alpha\alpha}^{(2)}(\mathbf{k}, E_{\mathbf{k}}) - \frac{B_{\mathbf{k}}^2}{2E_{\mathbf{k}}}\right]. \tag{18}$$

Expressions for the magnon Green's functions and self-energies are given in Appendix B.

We now define the renormalized spin-wave velocities along the x and y directions at the zone boundary using Eq. (18) as $V_x = \lim_{k_x\to 0} 2J_1 S(1+\zeta)\tilde{E}_{\mathbf{k}}^{\text{AF}}/k_x$ with $k_y = 0$ and $V_y = \lim_{k_y\to 0} 2J_1 S(1+\zeta)\tilde{E}_{\mathbf{k}}^{\text{AF}}/k_y$ with $k_x = 0$. The renormalization factors are expressed as

$$Z_{v_x}^{\text{AF}} \equiv \frac{V_x}{2J_1 S\sqrt{1+\zeta}} = v_{0x} + \frac{v_{1x}}{(2S)} + \frac{v_{2x}}{(2S)^2}, \tag{19}$$

$$Z_{v_y}^{\mathrm{AF}} \equiv \frac{V_y}{2J_1 S\sqrt{1+\zeta}} = v_{0y} + \frac{v_{1y}}{(2S)} + \frac{v_{2y}}{(2S)^2}, \tag{20}$$

where

$$v_{0x} = (1-2\eta)^{1/2}, \tag{21}$$

$$v_{1x} = (1-2\eta)^{-1/2}\left[(1-\eta)A_1 + \frac{1}{2}(1+\zeta)A_2\right], \tag{22}$$

$$v_{2x} = (1+\zeta)^{1/2}\lim_{k_x\to 0}\frac{1}{k_x}\left[\Sigma^{(2)}_{\alpha\alpha}(\mathbf{k},E_{\mathbf{k}}) - \frac{B_{\mathbf{k}}^2}{2E_{\mathbf{k}}}\right], \tag{23}$$

$$v_{0y} = (\zeta-2\eta)^{1/2}, \tag{24}$$

$$v_{1y} = (\zeta-2\eta)^{-1/2}\left[(\zeta-\eta)A_1 + \frac{1}{2}(1+\zeta)A_2\right], \tag{25}$$

$$v_{2y} = (1+\zeta)^{1/2}\lim_{k_y\to 0}\frac{1}{k_y}\left[\Sigma^{(2)}_{\alpha\alpha}(\mathbf{k},E_{\mathbf{k}}) - \frac{B_{\mathbf{k}}^2}{2E_{\mathbf{k}}}\right]. \tag{26}$$

The magnetization M defined as the average of the spin operator S_z on a given sublattice (say A) is expressed as

$$M = S - \langle a_i^\dagger a_i\rangle = S - \Delta S + \frac{M_1}{(2S)} + \frac{M_2}{(2S)^2}, \tag{27}$$

where

$$\Delta S = \frac{1}{N}\sum_{\mathbf{k}}\left(\frac{1}{\epsilon_{\mathbf{k}}} - 1\right), \tag{28}$$

$$M_1 = \frac{2}{N}\sum_{\mathbf{k}}\frac{l_{\mathbf{k}}m_{\mathbf{k}}B_{\mathbf{k}}}{E_{\mathbf{k}}}, \tag{29}$$

$$M_2 = \frac{2}{N}\sum_{\mathbf{k}}\left\{-(l_{\mathbf{k}}^2+m_{\mathbf{k}}^2)\frac{B_{\mathbf{k}}^2}{4E_{\mathbf{k}}^2} + \frac{l_{\mathbf{k}}m_{\mathbf{k}}}{E_{\mathbf{k}}}\Sigma^{(2)}_{\alpha\beta}(\mathbf{k},-E_{\mathbf{k}}) - \left(\frac{2}{N}\right)^2\sum_{\mathbf{pq}}2l_{\mathbf{k}}^2l_{\mathbf{p}}^2l_{\mathbf{q}}^2l_{\mathbf{k+p-q}}^2\left[\frac{(l_{\mathbf{k}}^2+m_{\mathbf{k}}^2)|V^{(6)}_{\mathbf{k},\mathbf{p},\mathbf{q},[\mathbf{k+p-q}]}|^2}{(E_{\mathbf{k}}+E_{\mathbf{p}}+E_{\mathbf{q}}+E_{\mathbf{k+p-q}})^2} + \frac{2l_{\mathbf{k}}m_{\mathbf{k}}\,\mathrm{sgn}(\gamma_{\mathbf{G}})V^{(4)}_{\mathbf{k},\mathbf{p},\mathbf{q},[\mathbf{k+p-q}]}V^{(6)}_{\mathbf{k},\mathbf{p},\mathbf{q},[\mathbf{k+p-q}]}}{E_{\mathbf{k}}^2-(E_{\mathbf{p}}+E_{\mathbf{q}}+E_{\mathbf{k+p-q}})^2}.\right]\right\} \tag{30}$$

The zeroth-order term ΔS corresponds to the reduction in magnetization within LSWT, M_1 term corresponds to the first-order $1/S$ correction, and M_2 is the second-order correction.

B. CAF phase: Formalism

Hamiltonian

In the CAF phase up and down spins interact along the row directions (NN coupling) and also along the diagonals (NNN coupling) whereas up-up and down-down spins interact along the column direction (NN coupling). The Hamiltonian for this phase is described by

$$H = J_1\sum_i \mathbf{S}_i^{\mathrm{A}}\cdot\mathbf{S}_{i+\delta_x}^{\mathrm{B}} + \frac{1}{2}J_1'\sum_i[\mathbf{S}_i^{\mathrm{A}}\cdot\mathbf{S}_{i+\delta_x+\delta_y}^{\mathrm{A}} + \mathbf{S}_i^{\mathrm{B}}\cdot\mathbf{S}_{i+\delta_x+\delta_y}^{\mathrm{B}}] + J_2\sum_i \mathbf{S}_i^{\mathrm{A}}\cdot\mathbf{S}_{i+\delta_y}^{\mathrm{B}}. \tag{31}$$

The Hamiltonians for the AF and the CAF ordered phases [Eqs. (3) and (31)] show the similarity between these two phases. In the AF phase J_2 interactions play the role of J_1' interactions in the CAF phase. For the CAF phase the structure factors $\gamma_{1\mathbf{k}}'$, $\gamma_{2\mathbf{k}}'$ along with other quantities required for the calculations are defined as

$$\gamma_{1\mathbf{k}}' = \{\cos(k_x)[1+2\eta\cos(k_y)]\}/(1+2\eta),$$

$$\gamma_{2\mathbf{k}}' = \cos(k_y),$$

$$\gamma_{\mathbf{k}}' = \gamma_{1\mathbf{k}}'/\kappa_{\mathbf{k}}',$$

$$\kappa_{\mathbf{k}}' = 1 - \frac{\zeta}{1+2\eta}(1-\gamma_{2\mathbf{k}}'),$$

$$\epsilon_{\mathbf{k}}' = [1-\gamma_{\mathbf{k}}'^2]^{1/2}. \tag{32}$$

The coefficients for the Oguchi correction that appear in the Hamiltonian H_1 are

$$A_{\mathbf{k}}' = A_1'\frac{1}{\kappa_{\mathbf{k}}'\epsilon_{\mathbf{k}}'}[\kappa_{\mathbf{k}}' - \gamma_{1\mathbf{k}}'^2] + A_2'\frac{1}{\epsilon_{\mathbf{k}}'}[1-\gamma_{2\mathbf{k}}'^2], \tag{33}$$

$$B_{\mathbf{k}}' = B_1'\frac{1}{\kappa_{\mathbf{k}}'\epsilon_{\mathbf{k}}'}\gamma_{1\mathbf{k}}'[1-\gamma_{2\mathbf{k}}'] \tag{34}$$

with

$$A_1' = \frac{2}{N}\sum_{\mathbf{p}}\frac{1}{\epsilon_{\mathbf{p}}'}\left[\frac{\gamma_{1\mathbf{p}}'^2}{\kappa_{\mathbf{p}}'} + \epsilon_{\mathbf{p}}' - 1\right], \tag{35}$$

$$A_2' = \left(\frac{\zeta}{1+2\eta}\right)\frac{2}{N}\sum_{\mathbf{p}}\frac{1}{\epsilon_{\mathbf{p}}'}[1-\epsilon_{\mathbf{p}}'-\gamma_{2\mathbf{p}}'], \tag{36}$$

$$B_1' = \left(\frac{\zeta}{1+2\eta}\right)\frac{2}{N}\sum_{\mathbf{p}}\frac{1}{\epsilon_{\mathbf{p}}'}\left[\gamma_{2\mathbf{p}}' - \frac{\gamma_{1\mathbf{p}}'^2}{\kappa_{\mathbf{p}}'}\right]. \tag{37}$$

H_0, H_1, and H_2 can be expressed in the same forms as in Eqs. (9), (10), and (17) with the new coefficients $A_{\mathbf{k}}', B_{\mathbf{k}}', C_{1\mathbf{k}}', C_{2\mathbf{k}}'$ and with the replacement $\zeta \leftrightarrow 2\eta$. The expressions for the two vertex factors $V'^{(4)}, V'^{(6)}$ and the coefficients $C_{1\mathbf{k}}', C_{2\mathbf{k}}'$ are given in Appendix C. As an example for the CAF phase Eq. (9) takes the form

$$H_0 = J_1 Sz(1+2\eta)\sum_{\mathbf{k}}\kappa_{\mathbf{k}}'(\epsilon_{\mathbf{k}}'-1) + J_1 Sz(1+2\eta)\sum_{\mathbf{k}}\kappa_{\mathbf{k}}'\epsilon_{\mathbf{k}}'(\alpha_{\mathbf{k}}^{\dagger}\alpha_{\mathbf{k}} + \beta_{\mathbf{k}}^{\dagger}\beta_{\mathbf{k}}). \tag{38}$$

The quasiparticle energy $\tilde{E}_{\mathbf{k}}^{\mathrm{CAF}}$ for magnon excitations, measured in units of $J_1 Sz(1+2\eta)$ up to second order in $1/S$ is given as

$$\tilde{E}_{\mathbf{k}}^{\mathrm{CAF}} = E_{\mathbf{k}}' + \frac{1}{2S}A_{\mathbf{k}}' + \frac{1}{(2S)^2}\left[\Sigma_{\alpha\alpha}'^{(2)}(\mathbf{k},E_{\mathbf{k}}') - \frac{B_{\mathbf{k}}'^2}{2E_{\mathbf{k}}'}\right]. \tag{39}$$

The renormalized spin-wave velocities along the x and y directions for this phase are defined as $V_x = \lim_{k_x\to 0} 2J_1 S(1+2\eta)\tilde{E}_{\mathbf{k}}^{\mathrm{CAF}}/k_x$ with $k_y=0$ and $V_y = \lim_{k_y\to 0} 2J_1 S(1+2\eta)\tilde{E}_{\mathbf{k}}^{\mathrm{CAF}}/k_y$ with $k_x=0$. The renormalization factors are

$$Z_{v_x}^{\mathrm{CAF}} \equiv \frac{V_x'}{2J_1 S(1+2\eta)} = v_{0x}' + \frac{v_{1x}'}{(2S)} + \frac{v_{2x}'}{(2S)^2}, \tag{40}$$

$$Z_{v_y}^{\mathrm{CAF}} \equiv \frac{V_y'}{2J_1 S(1+2\eta)} = v_{0y}' + \frac{v_{1y}'}{(2S)} + \frac{v_{2y}'}{(2S)^2}, \tag{41}$$

where

$$v_{0x}' = 1, \tag{42}$$

$$v_{1x}' = A_1', \tag{43}$$

$$v_{2x}' = \lim_{k_x\to 0}\frac{1}{k_x}\left[\Sigma_{\alpha\alpha}'^{(2)}(\mathbf{k},E_{\mathbf{k}}') - \frac{B_{\mathbf{k}}'^2}{2E_{\mathbf{k}}'}\right], \tag{44}$$

$$v_{0y}' = (2\eta+1)^{-1/2}(2\eta-\zeta)^{1/2}, \tag{45}$$

$$v_{1y}' = (2\eta+1)^{-1/2}(2\eta-\zeta)^{-1/2}\left[\left(2\eta-\frac{\zeta}{2}\right)A_1 + \frac{1}{2}(2\eta+1)A_2\right], \tag{46}$$

$$v_{2y}' = \lim_{k_y\to 0}\frac{1}{k_y}\left[\Sigma_{\alpha\alpha}'^{(2)}(\mathbf{k},E_{\mathbf{k}}') - \frac{B_{\mathbf{k}}'^2}{2E_{\mathbf{k}}'}\right], \tag{47}$$

III. RESULTS

A. AF phase

1. Spin-wave energy dispersion

We numerically evaluate Eq. (18) to obtain the spin-wave energy $2J_1 S(1+\zeta)\tilde{E}_{\mathbf{k}}^{\mathrm{AF}}$ as a function of momentum for several values of ζ and η. For the numerical summation, the first BZ is divided into N_L^2 meshes with $N_L=64$ and then 4096 points of $\mathbf{p}$ and 4096 points of $\mathbf{q}$ are summed up to evaluate the third term in Eq. (18). For some of the cases we have used $N_L=96$ for better accuracies.

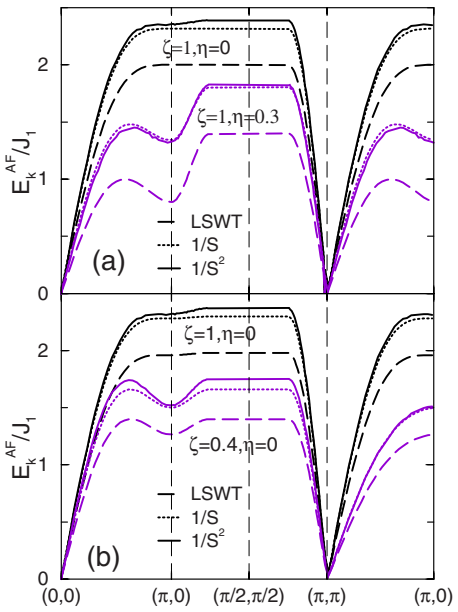

FIG. 2. (Color online) Spin-wave energy $E_{\mathbf{k}}^{\mathrm{AF}}/J_1$ obtained from LSWT (long-dashed lines) with first-order (dotted lines) and second-order corrections (solid lines) for the AF-ordered phase. Panel (a) is for isotropic coupling $\zeta=1$ with $\eta=0$ and $\eta=0.3$ and panel (b) is for $\eta=0$ (no frustration) and with two different values of anisotropy parameter $\zeta=1$ and 0.4. Both the first and second order corrections make the spin-wave energy larger and the corrections from LSWT (long-dashed lines) are significant in the entire BZ.

Figure 2 shows a comparison between the results from LSWT (long-dashed lines), first-order (dotted lines), and second-order corrections (solid lines) to the spin-wave energy. Figure 2(a) shows the spin-wave energies for isotropic coupling ($\zeta=1$) with $\eta=0$ and $\eta=0.3$ and Fig. 2(b) shows the results with two different values of anisotropy parameter $\zeta=1$ and 0.4 for $\eta=0$. We find that in the entire BZ both the first (dotted lines) and second order corrections (solid lines) make the spin-wave energy larger, and the corrections from LSWT (long-dashed lines) are significant for all cases.

In Fig. 3 we show the spin-wave energy results with second-order corrections for different values of ζ and η. The spin-wave energy curve for the isotropic coupling $\zeta=1$ with $\eta=0$ was reported earlier.[15] The dispersion along $(\pi/2,\pi/2)-(\pi,0)$ is flat within LSWT and $1/S$ correction (see Fig. 2 for example). The second-order corrections make the excitation energies at $(\pi,0)$ smaller than the energies at $(\pi/2,\pi/2)$. Our results for spin-wave energy with frustration and with anisotropic couplings are different. The dip in the magnon energy at $(\pi,0)$ increases with increase in frustration η. Experimentally this can provide a measure of the strength of NNN frustration.

In Fig. 4 we show the effect of the directional anisotropy parameter ζ on the spin-wave energy (with second-order cor-

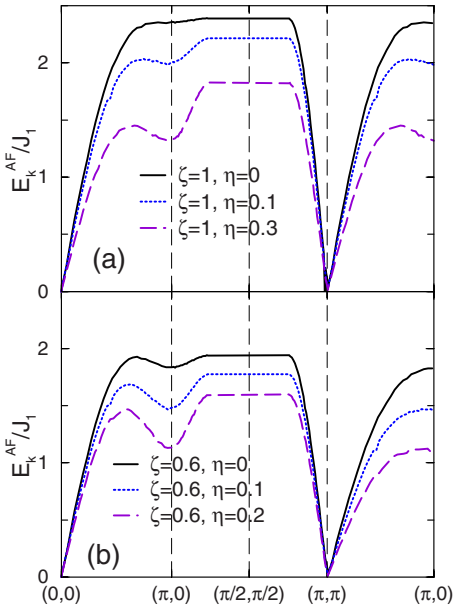

FIG. 3. (Color online) Spin-wave energy $E_{\mathbf{k}}^{\mathrm{AF}}/J_1$ for the AF ordered phase with second-order corrections is plotted for different values of ζ and η. The dispersion along $(\pi/2,\pi/2)-(\pi,0)$ is flat within LSWT and $1/S$ correction. The second-order corrections make the excitation energies at $(\pi,0)$ smaller than the energies at $(\pi/2,\pi/2)$ for all cases. With increase in NNN frustration η (for a fixed value of the directional parameter ζ) the dip in the magnon energy at $(\pi,0)$ increases. This can provide a measure of the strength of NNN frustration.

rections). Similar to Fig. 3 we find that the dip in the energy at $(\pi,0)$ increasing values of ζ.

Recently using neutron scattering measurements on copper deuteroformate tetradeurate (CFTD), a real two dimensional Heisenberg AF with weak interplane interactions $(\approx 10^{-5}-10^{-4}J_1)$ magnon energies have been obtained for the entire BZ.[2,3] It was found that the energies at $(\pi,0)$ is 13.5180 meV (with estimated error of 0.1641 meV), which is about 7(1)% smaller than the energy 14.4880 meV (with estimated error of 0.0647 meV) at $(\pi/2,\pi/2)$.[3,62] The coupling J_1 is estimated to be 6.19 meV. This local minimum at $(\pi,0)$ is due to quantum fluctuations and may be due to multimagnon processes (entanglement of spins on neighboring sites)

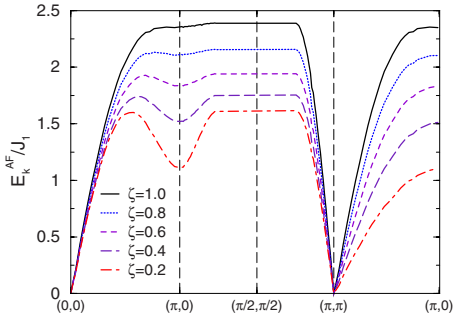

FIG. 4. (Color online) Effect of directional anisotropy parameter ζ on the spin-wave energy. The calculated spin-wave energy is with second-order corrections. Similar to Fig. 3 the dip in the energy at $(\pi,0)$ increases with increase in the values of ζ.

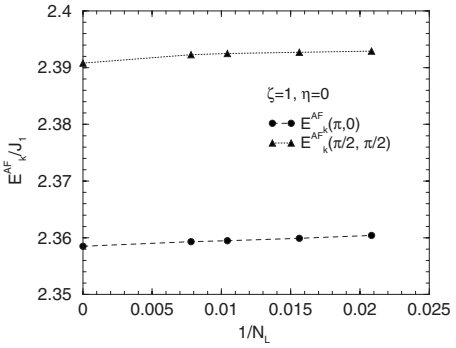

FIG. 5. Convergence of $E_{(\pi,0)}^{\mathrm{AF}}/J_1$ and $E_{(\pi/2,\pi/2)}^{\mathrm{AF}}/J_1$ is shown with $1/N_L$ for N_L=48, 64, 96, and 128. We extrapolate these results using the fitting function $A+B/N_L+C/N_L^2+D/N_L^3$ to obtain $E_{(\pi,0)}^{\mathrm{AF}}/J_1=2.3585$, $E_{(\pi/2,\pi/2)}^{\mathrm{AF}}/J_1=2.3908$ for $N_L\to\infty$.

at this zone boundary. Series expansion around the Ising limit[38] and quantum Monte Carlo methods[47] have accounted for all of the experimental data. But these numerical methods do not provide any insight into the physics at this zone boundary. To test our numerical procedure we systematically calculate the values of $E_{(\pi,0)}^{\mathrm{AF}}/J_1$ and $E_{(\pi/2,\pi/2)}^{\mathrm{AF}}/J_1$ for N_L=36, 48, 64, 96, and 128. The convergence of our results are very good as shown in Fig. 5. We extrapolate these results using the fitting function $A+B/N_L+C/N_L^2+D/N_L^3$ to obtain A for $N_L\to\infty$ and reproduce the numerical results $E_{(\pi,0)}^{\mathrm{AF}}/J_1 \approx 2.3585$, $E_{(\pi/2,\pi/2)}^{\mathrm{AF}}/J_1\approx 2.3908$ reported earlier[15] with a 1.4% decrease between these two energy values. Recently a third order in $1/S$ expansion has been done to obtain the spectrum of short-wavelength magnons[23,63] where it was shown that the $1/S$ series converges slowly near the wave vector $(\pi,0)$. With the third order correction the excitation energy at $(\pi,0)$ was found to be 3.2% smaller than at $(\pi/2,\pi/2)$. This result for the energy difference still falls short of the experimental result of 7%. This suggests that the inclusion of correction to even third order in $1/S$ is insufficient to explain this energy difference. It should be noted that other interactions, e.g., ring exchange interactions have been proposed to play a role in these compounds.[9,64,65]

It may be interesting to study the effects of small NNN frustration and small anisotropy on the energies at these two zone boundaries. Table I shows our extrapolated values of $E_{(\pi,0)}^{\mathrm{AF}}/J_1$ and $E_{(\pi/2,\pi/2)}^{\mathrm{AF}}/J_1$ and the percentage changes for small frustrations η=0.01, 0.02 and a small directional anisotropy ζ=0.98. Calculations are done with lattice sizes N_L =48, 64, 96, and 128 and the results are extrapolated to $N_L\to\infty$ using the fitting function $A+B/N_L+C/N_L^2+D/N_L^3$. We show that a small frustration (for example, η=0.02) for the isotropic coupling causes a noticeable difference (2.8% within second-order spin-wave expansion) in energies between $E_{(\pi,0)}^{\mathrm{AF}}/J_1$ and $E_{(\pi/2,\pi/2)}^{\mathrm{AF}}/J_1$. These features can be explored experimentally using neutron scattering measurements with compounds that can be modeled by the J_1-J_1'-J_2 Heisenberg antiferromagnet.

2. Renormalized spin-wave velocities

We calculate the spin-wave velocity renormalization factors $Z_{v_x}^{\mathrm{AF}}, Z_{v_y}^{\mathrm{AF}}$ along the x and y directions from Eq. (20). For

TABLE I. Energies $E^{\mathrm{AF}}_{(\pi,0)}/J_1$ and $E^{\mathrm{AF}}_{(\pi/2,\pi/2)}/J_1$ for different values of ζ and η.

$N_L\to\infty$		$E^{\mathrm{AF}}_{(\pi,0)}/J_1$	$E^{\mathrm{AF}}_{(\pi/2,\pi/2)}/J_1$	$\Delta E^{\mathrm{AF}}/E^{\mathrm{AF}}_{(\pi/2,\pi/2)}$ (%)
$\zeta=1,\ \eta=0$	LSWT	2.0000	2.0000	0
	$1/S$	2.3159	2.3159	0
	$1/S^2$	2.3585	2.3908	1.4
$\zeta=1,\ \eta=0.01$	LSWT	1.9600	1.9800	1.0
	$1/S$	2.2800	2.2980	0.8
	$1/S^2$	2.3221	2.3753	2.2
$\zeta=1,\ \eta=0.02$	LSWT	1.9200	1.9600	2.0
	$1/S$	2.2443	2.2801	1.6
	$1/S^2$	2.2886	2.3536	2.8
$\zeta=0.98,\ \eta=0$	LSWT	1.9799	1.9800	0
	$1/S$	2.2926	2.2928	0
	$1/S^2$	2.3348	2.3680	1.4

the second-order correction terms v_{2x}, v_{2y}, we consider lattice size $N_L=72$ and evaluate $[\Sigma^{(2)}_{\alpha\alpha}(\mathbf{k},E_{\mathbf{k}})-\frac{B^2_{\mathbf{k}}}{2E_{\mathbf{k}}}]/k_x$ with $k_x=\pi/N_L$. v_{2y} is obtained similarly. For the isotropic case $\zeta=1$ and with $\eta=0$ we find the second-order correction $v_{2x}=v_{2y}=0.021$ which is in excellent agreement with results reported earlier.[14,15,21] The results from our calculations with increase in η are shown in Fig. 6. We find that the velocities steadily decrease with increase in frustration and finally becomes zero close to the quantum critical points η_{1c} for the AF phase. Second-order corrections are significant to stabilize the velocities as with first-order corrections these velocities diverge with increase in frustration (similar to the case

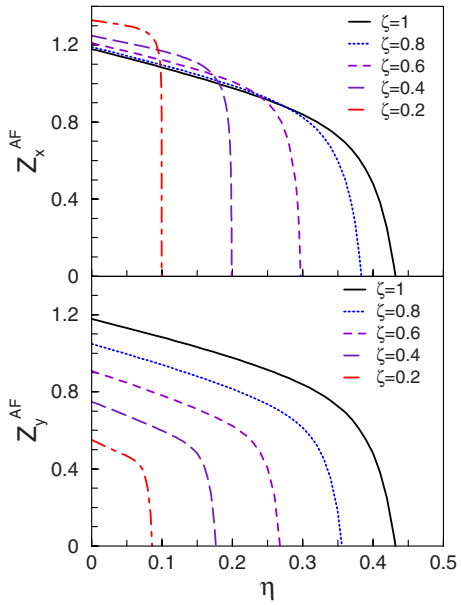

FIG. 6. (Color online) Renormalization factors $Z^{\mathrm{AF}}_{v_x}$ and $Z^{\mathrm{AF}}_{v_y}$ for the spin-wave velocities are plotted with frustration η for different values of ζ. The velocities steadily decrease with increase in NNN frustration and finally becomes zero close to the quantum critical transition points η_{1c} for the AF-phase.

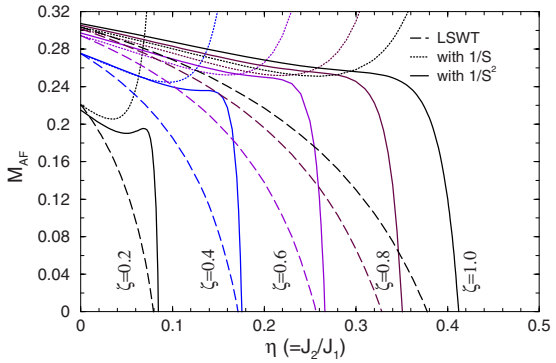

FIG. 7. (Color online) Staggered magnetization M_{AF} is shown for the AF ordered phase with frustration $\eta=J_2/J_1$ with different values of spatial anisotropy $\zeta=J_1'/J_1$. For each ζ results from LSWT (long-dashed lines), with first-order (dotted lines) and with second-order corrections (solid lines) are plotted. With increase in η the dotted curves diverge. Second-order $1/S^2$ corrections become significant for large η and they stabilize the apparent divergence of the magnetization. Magnetizations with $1/S^2$ corrections decrease steadily and then sharply drop to zero. For example in the isotropic case i.e. $\zeta=1$, M_{AF} starts from 0.307 and then decreases till $\eta\approx0.32$ and finally becomes zero at the critical point $\eta_{1c}\approx0.41$. However for small ζ, say $\zeta=0.2$ we find M_{AF} to steadily decrease from 0.21 at $\eta=0$–0.19 at $\eta\approx0.054$ and then slightly increases to 0.195 at $\eta\approx0.068$. Finally it sharply drops to zero at $\eta_{1c}\approx0.084$. Note that for all cases second-order corrections increase the critical value of η_{1c} from the LSWT predictions.

with magnetization discussed later). We also notice that the difference between the renormalization factors $Z^{\mathrm{AF}}_{v_x}$ and $Z^{\mathrm{AF}}_{v_y}$ diminishes with increase in frustration.

3. *Staggered magnetization*

We obtain the staggered magnetization M_{AF} for the AF phase with several values of ζ and η from Eq. (27) by numerically evaluating Eqs. (28)–(30). Especially to obtain the second order correction term M_2 we sum up the values of $N_L^2/4$ points of $\mathbf{k}$ in the 1/4 part of the first BZ and N_L^2 points of $\mathbf{p}$ and $\mathbf{q}$ in the first BZ with $N_L=36$ lattice sites (total of about 544.2 million points for each ζ and η). Except for small spatial anisotropy ζ, M_2 values start from a positive small number and then switch sign and become negative with increase in frustration η. However, for small ζ, say $\zeta=0.2$ M_2 starts from a small negative number (~-0.005) and remains negative with increase in η. Figure 7 shows the magnetization with increase in the frustration parameter $\eta=J_2/J_1$ for several values of the spatial anisotropy parameter $\zeta=J_1'/J_1=0.2$, 0.4, 0.6, 0.8, and 1.0. For each ζ three different curves are plotted: the long-dashed lines represent LSWT prediction, the dotted lines include the first-order $(1/S)$ correction to the LSWT results and the solid lines represent corrections up to second-order $(1/S^2)$ to the LSWT results. With increase in frustration the dotted curves diverge. However, $1/S^2$ corrections (M_2) significantly increase with frustration and stabilize the apparent divergence of the magnetization. We find that the magnetization with second-order corrections decreases steadily at first and then sharply drops to zero. As an example, for the isotropic case $(\zeta=1,\ \eta=0)$,

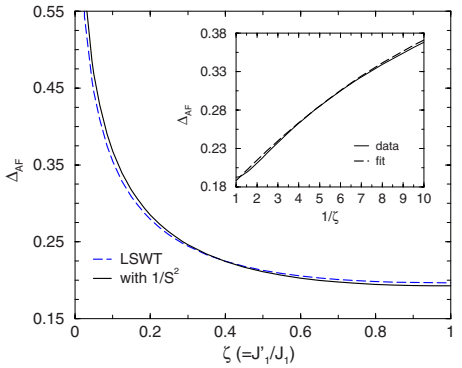

FIG. 8. (Color online) Spin deviation $\Delta_{AF}=0.5-M_{AF}^{(0)}$ from the classical value of 0.5 is plotted for the AF ordered phase (with no NNN interaction, i.e. $\eta=0$) for different values of spatial anisotropy ζ. Dashed line is LSWT prediction whereas the solid line includes $1/S^2$ corrections to LSWT results. The fluctuation increases with decreasing values of ζ, suggesting that spin-wave expansion for $S=\frac{1}{2}$ is unreliable for $\zeta<0.1$. In the inset we show the fluctuations with $1/\zeta$ for $\zeta=0.1-1$. The function $f(\zeta)=0.16+0.029\zeta^{-1}-0.00079\zeta^{-2}$ is a good representation of Δ_{AF} for $\zeta=0.1-1.0$. The fitted curve is shown in the inset along with the actual numerical results with the second-order corrections.

M_{AF} starts from 0.307 and then decreases till $\eta\approx0.32$ and finally becomes zero at the critical point $\eta_{1c}\approx0.41$. For this case we reproduce the magnetization plot obtained in Ref. 13. Other values of ζ show the same trend except for small ζ. For $\zeta=0.2$ we find M_{AF} steadily decreases from 0.21 at $\eta=0$ to 0.19 at $\eta\approx0.054$ and then slightly increases to 0.195 at $\eta\approx0.068$. Finally it sharply drops to zero at $\eta_{1c}\approx0.084$. This feature has not been observed before and may be an artifact of the spin-wave expansion showing the limitation of this method for small ζ (the system becomes essentially one-dimensional as $\zeta\to0$). It may be interesting to verify this by series expansion or other analytical or numerical methods. Note that for all cases second-order corrections increase the critical value of η_{1c} from the LSWT predictions. Our values of magnetization for $\eta=0$ (no NNN frustration), $M_{AF}^{(0)}=0.307$ agrees with previously obtained values from spin-wave expansion,[13–15,66] series expansion,[33–37] and experimental results for K_2NiF_4, K_2MnF_4, Rb_2MnF_4, and other systems.[3,8–11]

The ground-state magnetization per spin is reduced from its classical value $S=1/2$ by zero-point quantum fluctuations. This "spin reduction" $\Delta_{AF}=0.5-M_{AF}^{(0)}$ is plotted for different values of ζ for $\eta=0$ in Fig. 8. Second-order corrections (solid line) change the values of $M_{AF}^{(0)}$ slightly from the LSWT predictions (dashed line). The fluctuations increase with decreasing values of ζ, suggesting that spin-wave expansion for $S=1/2$ is not applicable for $\zeta<0.1$ as the system essentially becomes one dimensional.

In the inset of Fig. 8 we show the spin deviation with $1/\zeta$ for $\zeta=0.1-1$. We find that the function $f(\zeta)=0.16+0.029\zeta^{-1}-0.00079\zeta^{-2}$ is a good representation of Δ_{AF} for this range of ζ. The fitted curve (dashed line) is shown in the inset along with the actual numerical results (solid line) with the second-order corrections.

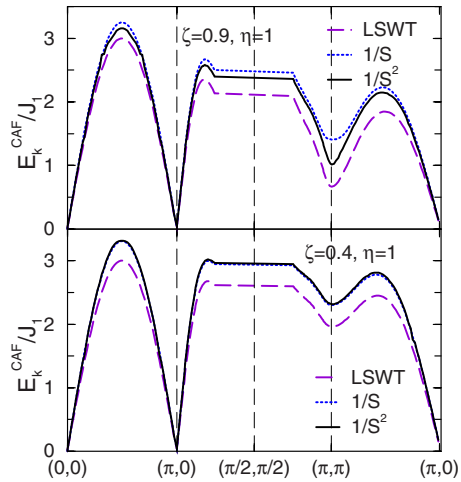

FIG. 9. (Color online) Spin-wave energy $E_{\mathbf{k}}^{CAF}/J_1$ results obtained from linear spin-wave theory (long-dashed lines), with first-order (dotted lines), and second-order corrections (solid lines) for the entire Brillouin zone of the CAF-ordered phase. For fixed NNN frustration $\eta=1$ two different values of $\zeta=0.9$ and 0.4 are chosen. $1/S$ and $1/S^2$ corrections increase the spin-wave energy of the ordered phase from the linear-spin wave theory results. For $\zeta=0.4$ second order corrections are insignificant compared to the first order $1/S$ corrections. However, for $\zeta=0.91/S^2$ corrections lower the spin-wave energy from the first-order corrections. Spin-wave energy shows three peaks, the maximum being at $(\pi/2,0)$. The second small peak is at $(0.514\pi,0.486\pi)$ and the third peak occurs at $(\pi,\pi/2)$.

B. CAF phase

1. Spin-wave energy dispersion

We numerically evaluate Eq. (39) with $N_L=72$ lattice size to obtain the spin-wave energy $2J_1S(1+2\eta)\tilde{E}_{\mathbf{k}}^{CAF}$ as a function of momentum for several values of ζ and η. The calculations are similar to the AF phase. Figure 9 shows the spin-wave energy $\tilde{E}_{\mathbf{k}}^{CAF}/J_1$ with second-order corrections (solid lines) for the entire Brillouin zone of the CAF-ordered phase. Two different values of directional anisotropy $\zeta=0.9$ and 0.4 for NNN frustration $\eta=1$ are chosen. Results obtained from linear spin-wave theory (long-dashed lines) and with only first-order (dotted lines) are also shown for comparison. $1/S$ and $1/S^2$ corrections increase the energy of the ordered phase from the LSWT results. We find that the second-order corrections to the magnon energy are not significant from the energy obtained with first-order corrections for small ζ. However for large ζ, say $\zeta=0.9$ $1/S^2$ corrections lower the spin-wave energy from the first-order $1/S$ corrections.

Figure 10 shows the effect of frustration η for a fixed value of spatial anisotropy $\zeta=0.6$. Second-order corrections are negligible compared to the first-order corrections, which significantly enhance the LSWT results. In both Figs. 9 and 10 the spin-wave energy vanishes at the wave vector $(\pi,0)$ as expected for the CAF phase. We find three peaks in the magnon energy, the maximum being at $(\pi/2,0)$. The second small peak in energy is at $(0.514\pi,0.486\pi)$ and the third peak occurs at $(\pi,\pi/2)$.

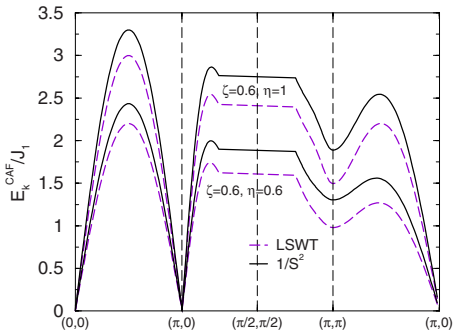

FIG. 10. (Color online) Effect of frustration η on the spin-wave energy in the CAF-phase. Second-order corrections are negligible compared to the first-order corrections. However, $1/S$ corrections significantly enhance the spin-wave energy obtained from LSWT results.

2. Renormalized velocities

Renormalization factors $Z_{v_x}^{\mathrm{CAF}}, Z_{v_y}^{\mathrm{CAF}}$ along the x and y directions are obtained from Eq. (41) with second-order corrections. The results are shown in Fig. 11. As we expect similar to the AF phase the velocities steadily decrease with increase in η and finally becomes zero close to the quantum transition points η_{2c} for the CAF phase. Second-order corrections are significant to stabilize the velocities as with first-order corrections these velocities diverge with increase in frustration (similar to the case with magnetization discussed later). For small ζ (ζ=0.2,0.4 in figure) we find that $Z_{v_x}^{\mathrm{CAF}}$ slightly increases and then sharply drops to zero. We increase the lattice size to N_L=96 to check the accuracy of our calculation. We find no changes in our plot. It may be interesting to verify this with series expansion or other analytical or numerical methods. Our numerical method based on the spin-wave expansion for the CAF phase is not reliable for $\zeta > 0.95$—so we have not been able to obtain the renormalized spin-wave velocities for the case with ζ=1 and η=1 (more discussed in Sec. III B 3).

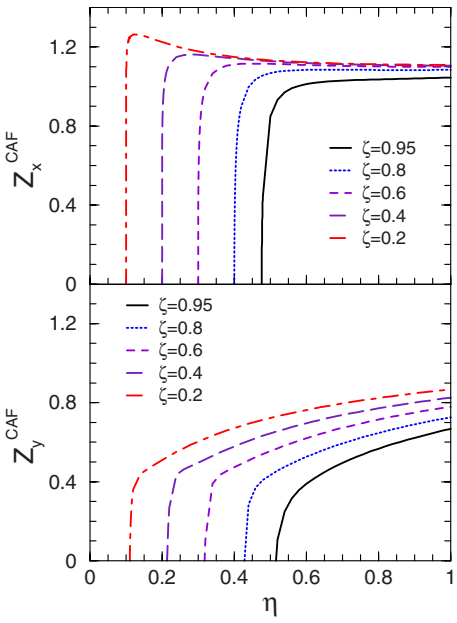

FIG. 11. (Color online) Renormalization factors $Z_{v_x}^{\mathrm{CAF}}$ and $Z_{v_y}^{\mathrm{CAF}}$ are plotted with frustration η for different values of ζ. The velocities steadily decrease with increase in NNN frustration and finally become vanish close to the quantum critical transition points η_{2c} for the CAF phase. Numerical calculations are done with lattice size N_L=72. For ζ=0.2,0.4 we find that $Z_{v_x}^{\mathrm{CAF}}$ slightly increases and then sharply drops to zero. Increasing the lattice size to N_L=96 does not change our results.

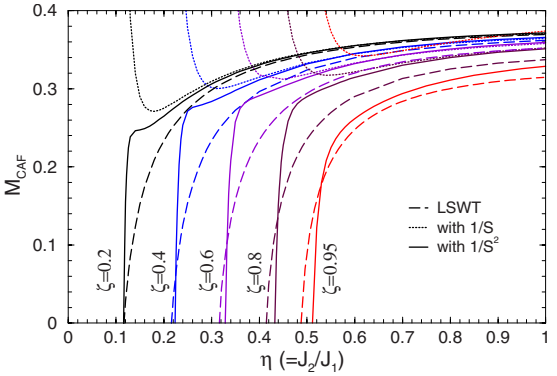

FIG. 12. (Color online) Staggered magnetization M_{CAF} for the CAF ordered phase is plotted with η for different values of ζ. For each value of ζ three different curves are shown: long-dashed line is the prediction from LSWT, dotted line is the first-order correction, and the solid line includes corrections up to second order. In all cases first-order corrections diverge for some value of η. However, second-order $(1/S^2)$ corrections become significant and stabilize the magnetization. Similar to the AF phase M_{CAF} with second-order corrections decreases steadily and then sharply drops to zero. For example, with ζ=0.2, M_{CAF} starts from 0.371 at η=1 and then decreases till $\eta \approx 0.12$ and sharply drops to zero at the critical point $\eta_{2c} \approx 0.116$. For ζ more than 0.95 the fluctuations become too large (see Fig. 13)—in that case our spin-wave expansion becomes invalid (see text). With increase in ζ the values of the critical points η_{2c} differ more from the LSWT predictions.

3. Staggered magnetization

Similar to the AF phase the staggered magnetization M_{CAF} for the CAF phase with several values of ζ and η are obtained by summing over points in the first BZ with N_L =36 lattice sites. Except for large spatial anisotropy ζ, M_2 values start from a small positive number and then switches sign and become negative with increase in frustration η. However, for large ζ, say for ζ=0.8 M_2 corrections are always negative. Figure 12 shows the magnetization with increase in frustration parameter η for several values of ζ =0.2, 0.4, 0.6, 0.8, and 0.95. For each ζ three different curves are plotted: LSWT results (long-dashed line), first-order corrections (dotted line), and second-order corrections (solid line) to the LSWT results. Similar to the AF phase the dotted curves diverge with increase in frustration. However, $1/S^2$ corrections (M_2) significantly increase with frustration and stabilize the magnetization and finally make it zero. We find that M_{CAF} decreases steadily at first and then sharply drops to zero. As an example, for the ζ=0.2 M_{CAF} starts from 0.371 and then decreases till $\eta \approx 0.12$ and sharply drops to zero at

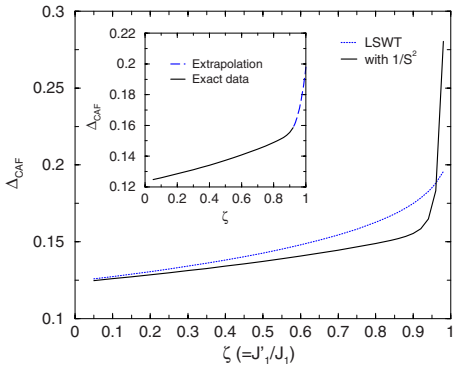

FIG. 13. (Color online) Spin deviation Δ_{CAF} is plotted for the CAF-ordered phase ($\eta=1$). Dashed line is LSWT results and the solid line is with the $1/S^2$ corrections. For ζ more than 0.95 spin-wave expansion becomes unreliable as Δ_{CAF} as the first and second-order corrections to Δ_{CAF} increase rapidly. Thus with the $1/S^2$ corrections we extrapolated the values to obtain $\Delta_{\mathrm{CAF}}\approx 0.20$ for $\zeta=1$. This gives $M_{\mathrm{CAF}}\approx 0.30$ for the isotropic limit. This is in good agreement with existing experimental results (see text). Inset shows both the exact data (solid line) and the extrapolated curve (dashed line).

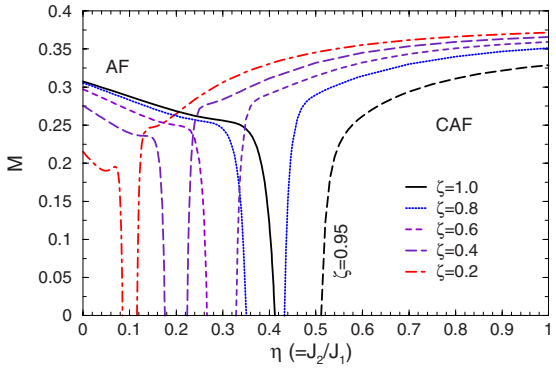

FIG. 14. (Color online) Staggered magnetization M is plotted for both the AF- and CAF-ordered phase (with second-order corrections). For the AF phase the different values of ζ are 0.2, 0.4, 0.6, 0.8, and 1.0 and for the CAF phase the values are 0.2, 0.4, 0.6, 0.8, and 0.95. Our numerical approach using spin-wave expansion is not reliable for the CAF phase for ζ larger than 0.95 (see text for details). For both the phases M become zero at some critical values of the NNN frustration parameter η. We also find that the spin-gap increases with increase in η.

the critical point $\eta_{2c}\approx 0.116$. With increase in ζ the values of the critical points η_{2c} differ more from LSWT predictions.

We also find that starting from $\zeta=0.95$ the spin deviation $\Delta_{\mathrm{CAF}}=0.5-M^{(0)}_{\mathrm{CAF}}$ increases substantially as we approach the isotropic limit $\zeta=1$. This is shown in Fig. 13. Δ_{CAF} from the LSWT theory remains smooth (dashed lines in Fig. 13). Both the first (M_1) and second order (M_2) corrections increase rapidly for $\zeta>0.95$. This increase is due to the fact that $\epsilon'_{\mathbf{k}}\rightarrow 0$ as $\zeta\rightarrow 1$. We have not found a numerical way to regulate it. Instead we used extrapolation to obtain values of Δ_{CAF} beyond $\zeta=0.95$. Inset of Fig. 13 shows both the exact data (solid line) and the extrapolated curve (dashed line). With the extrapolated curve we obtain $\Delta_{\mathrm{CAF}}\approx 0.20$ for $\zeta=1$, which gives $M_{\mathrm{CAF}}\approx 0.30$ for the isotropic limit. This is in good agreement with the recent neutron-scattering-measurements data of the order parameter $M_{\mathrm{CAF}}=0.31(2)$ for Li_2VOSiO_4, which is believed to be a $S=1/2$ frustrated antiferromagnet on a square lattice with $J_2\approx J_1$.[4–7]

C. AF and CAF ordered phases: Phase diagram

Staggered magnetizations of a spatially anisotropic frustrated spin-$\frac{1}{2}$ Heisenberg antiferromagnet on a square lattice is presented in Fig. 14 for both AF and CAF ordered phases. We find the staggered magnetization $M^{(0)}_{\mathrm{AF}}$ for $\eta=0$ to decrease with decrease in anisotropy ζ in the AF phase. On the other hand, $M^{(0)}_{\mathrm{CAF}}$ increases with decrease in ζ for $\eta=1$. Our results for $M^{(0)}_{\mathrm{AF}}=0.307$ for the AF-ordered phase and $M^{(0)}_{\mathrm{CAF}}=0.30$ for the CAF-ordered phase are in excellent agreement with existing experimental data on these systems. Furthermore, we find that in both the phases the second-order corrections play a significant role to stabilize the magnetization. Staggered magnetizations become zero in both the phases at the critical values η_{1c} and η_{2c} for each value of ζ.

Phase diagram for the J_1-J'_1-J_2 model is displayed in Fig. 15. The solid lines indicate the critical points η_{1c} for the AF and η_{2c} for the CAF phases. The dashed line is the classical first-order phase transition line between the two phases. Our spin-wave expansion for the CAF phase becomes unreliable for $\eta>0.95$. Thus we extrapolate our data to obtain $\eta_{2c}=0.58$ for $\zeta=1$. The dotted line in Fig. 15 is the extrapolated curve. This result $\eta_{2c}=0.58$ is in good agreement with the expected value of ≈ 0.60 for the isotropic case. Figure 15 shows that the spin gap $(\eta_{2c}-\eta_{1c})$ increases with increase in ζ.

Within our spin-wave expansion we do not find any quantum triple point for any values of ζ and η. This is in contrary to the findings in Refs. 43–45. Instead from our calculations we find that there are two ordered phases separated by the magnetically disordered phase. Our proposed phase diagram is consistent with the phase diagram obtained by the DMRG

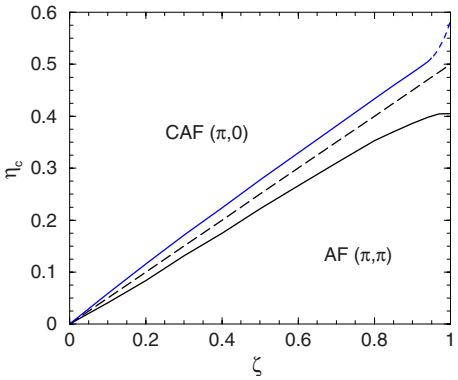

FIG. 15. (Color online) Phase diagram for the J_1-J'_1-J_2 model. The solid lines indicate the critical points η_{1c} for the AF and η_{2c} for the CAF phases. Our spin-wave expansion for the CAF phase becomes unreliable for $\eta>0.95$. We extrapolate our data to find $\eta_{2c}=0.58$ for $\zeta=1$. The dotted line is the extrapolated curve. The dashed line in the middle represents the classical first-order phase transition line $\eta_c^{\mathrm{class}}=\zeta/2$. The spin gap $(\eta_{2c}-\eta_{1c})$ increases with the anisotropy parameter ζ.

calculations,[41] exact diagonalization method,[39] and the results from the continuum limit of the present model.[28] Our results are also in accord with the numerical evidence of a dimerized intermediate phase in the frustrated two leg model up to a certain value of the interchain coupling.[56,57]

IV. CONCLUSIONS

In this work for an antiferromagnetic square lattice we have provided a comprehensive study of the effects of quantum fluctuations due to spatial anisotropy and frustration between nearest and next-nearest neighbors on the low-temperature thermodynamic properties of the two ordered phases of the system. Using second-order spin-wave expansion we have calculated the spin-wave energy in the entire Brillouin zone, renormalized spin-wave velocities, and the magnetizations for the antiferromagnetic Neél and columnar antiferromagnetic phases. We have found that the second-order corrections contribute significantly to stabilize the quantum phase diagram of the system as frustration between the spins increase. As expected from linear spin-wave-theory magnetization becomes zero at the quantum-critical points. However, the second-order corrections slightly extend the region of the AF order.

Our results for the spin-wave energies are compared with the recent experimental results using neutron scattering for CFTD.[3] With our second-order spin-wave expansion we have reproduced the previous numerical results that the spin-wave energy at $(\pi,0)$ is about 1.4% smaller that at $(\pi/2,\pi/2)$. This result falls short of the experimental result. Furthermore, we find that the dip in spin wave energy at $(\pi,0)$ increases with increase in NNN frustration. This can provide a measure of the effect of frustration experimentally. For a few values of small frustration and anisotropy we have explicitly calculated the percentage changes between the spin-wave energies at $(\pi,0)$ and at $(\pi/2,\pi/2)$. We have shown how the renormalized spin-wave velocities along the row and column direction change with frustration. Both these velocities become zero close to the critical transition points. For the AF-ordered phase we have also calculated the spin deviation from the classical value of 0.5 with no NNN coupling for different values of directional anisotropies and have obtained an empirical equation based on our numerical data.

For the CAF-ordered phase we have obtained similar results. The magnetization becomes zero at the quantum-critical points as frustration increases. For $\zeta<0.95$ our calculations produce correct results but our present numerical approach is not reliable for $\zeta>0.95$. Thus we were not able to find the thermodynamic properties for $\zeta=1$. Based on our data we have extrapolated the magnetization for the case $\zeta=1$, $\eta=1$ and found it to be 0.30 which is in good agreement with existing experimental result.[4–7] Our extrapolated value of the quantum critical point $\eta_{2c}=0.58$ for $\zeta=1$, $\eta=1$ is also in good agreement with the expected value ≈ 0.60. We have not found much experimental data on this system to compare with our other results such as the spin-wave-energy dispersion in the entire BZ and the spin-wave velocities.

Finally we combined our results for the magnetization of the two phases with different directional anisotropies to obtain the complete magnetic phase diagram of the system. We have found that two ordered phases are always separated by the disordered paramagnetic phase. Our proposed phase diagram is consistent with the phase diagram obtained from the DMRG calculations,[41] exact diagonalization method,[39] and the results from the continuum limit of the present model.[28] Our results are also in accord with the numerical evidence of a dimerized intermediate phase in the frustrated two leg model up to a certain value of the interchain coupling. In summary with our present approach based on second-order spin-wave expansion we do not find existence of quantum triple points for any values of ζ and η.

ACKNOWLEDGMENTS

The author would like to thank M. Krćmar, C. J. Hamer, and A. L. Chernyshev for useful discussions and comments, and A. Genz, N. Woody for computational help. This project acknowledges the use of the Cornell Center for Advanced Computing's "MATLAB on the TeraGrid" experimental computing resource funded by NSF under Grant No. 0844032 in partnership with Purdue University, Dell, The MathWorks, and Microsoft.

APPENDIX A: VERTEX FACTORS FOR THE AF PHASE

The six vertex factors for the AF phase are given below.

$$
\begin{aligned}
V_{1234}^{(1)} &= \gamma_1(1-4)x_1x_4 + \gamma_1(1-3)x_1x_3 + \gamma_1(2-4)x_2x_4 + \gamma_1(2-3)x_2x_3 \\
&\quad - \frac{1}{2}[\gamma_1(1)x_1 + \gamma_1(2)x_2 + \gamma_1(3)x_3 + \gamma_1(4)x_4 + \gamma_1(2-3-4)x_2x_3x_4 \\
&\quad + \gamma_1(1-3-4)x_1x_3x_4 + \gamma_1(4-2-1)x_1x_2x_4 + \gamma_1(3-2-1)x_1x_2x_3] \\
&\quad - \left(\frac{2\eta}{1+\zeta}\right) f_{1234}[1 + \mathrm{sgn}(\gamma_{\mathbf{G}})x_1x_2x_3x_4],
\end{aligned}
\tag{A1}
$$

$$V^{(2)}_{1234} = \gamma_1(2-4)x_1x_3 + \gamma_1(1-4)x_2x_3 + \gamma_1(2-3)x_1x_4 + \gamma_1(1-3)x_2x_4$$
$$-\frac{1}{2}[\gamma_1(2)x_1x_3x_4 + \gamma_1(1)x_2x_3x_4 + \gamma_1(4)x_1x_2x_3 + \gamma_1(3)x_1x_2x_4$$
$$+ \gamma_1(2-3-4)x_1 + \gamma_1(1-3-4)x_2 + \gamma_1(4-2-1)x_3 + \gamma_1(3-2-1)x_4]$$
$$-\left(\frac{2\eta}{1+\zeta}\right)f_{1234}[x_1x_2x_3x_4 + \mathrm{sgn}(\gamma_{\mathbf{G}})], \tag{A2}$$

$$V^{(3)}_{1234} = \gamma_1(2-4) + \gamma_1(1-3)x_1x_2x_3x_4 + \gamma_1(1-4)x_1x_2 + \gamma_1(2-3)x_3x_4$$
$$-\frac{1}{2}[\gamma_1(2)x_4 + \gamma_1(1)x_1x_2x_4 + \gamma_1(2-3-4)x_3 + \gamma_1(1-3-4)x_1x_2x_3$$
$$+ \gamma_1(4)x_2 + \gamma_1(3)x_2x_3x_4 + \gamma_1(4-2-1)x_1 + \gamma_1(3-2-1)x_1x_3x_4]$$
$$-\left(\frac{2\eta}{1+\zeta}\right)f_{1234}[x_2x_4 + \mathrm{sgn}(\gamma_{\mathbf{G}})x_1x_3], \tag{A3}$$

$$V^{(4)}_{1234} = -\gamma_1(2-4)x_4 - \gamma_1(1-4)x_1x_2x_4 - \gamma_1(2-3)x_3 - \gamma_1(1-3)x_1x_2x_3$$
$$+\frac{1}{2}[\gamma_1(2) + \gamma_1(1)x_1x_2 + \gamma_1(3)x_2x_3 + \gamma_1(4)x_2x_4$$
$$+ \gamma_1(2-3-4)x_3x_4 + \gamma_1(1-3-4)x_1x_2x_3x_4 + \gamma_1(3-2-1)x_1x_3 + \gamma_1(4-2-1)x_1x_4]$$
$$+\left(\frac{2\eta}{1+\zeta}\right)f_{1234}[x_2 + \mathrm{sgn}(\gamma_{\mathbf{G}})x_1x_3x_4], \tag{A4}$$

$$V^{(5)}_{1234} = -\gamma_1(2-4)x_1 - \gamma_1(2-3)x_1x_3x_4 - \gamma_1(1-4)x_2 - \gamma 1018_1(1-3)x_2x_3x_4$$
$$+\frac{1}{2}[\gamma_1(2)x_1x_4 + \gamma_1(1)x_2x_4 + \gamma_1(4)x_1x_2 + \gamma_1(3)x_1x_2x_3x_4$$
$$+ \gamma_1(2-3-4)x_1x_3 + \gamma_1(1-3-4)x_2x_3 + \gamma_1(4-2-1) + \gamma_1(3-2-1)x_3x_4]$$
$$+\left(\frac{2\eta}{1+\zeta}\right)f_{1234}[x_1x_2x_4 + \mathrm{sgn}(\gamma_{\mathbf{G}})x_3], \tag{A5}$$

$$V^{(6)}_{1234} = \gamma_1(2-4)x_2x_3 + \gamma_1(2-3)x_2x_4 + \gamma_1(1-3)x_1x_4 + \gamma_1(1-4)x_1x_3$$
$$-\frac{1}{2}[\gamma_1(2)x_2x_3x_4 + \gamma_1(3)x_4 + \gamma_1(2-3-4)x_2 + \gamma_1(3-2-1)x_1x_2x_4$$
$$+ \gamma_1(1)x_1x_3x_4 + \gamma_1(4)x_3 + \gamma_1(1-3-4)x_1 + \gamma_1(4-2-1)x_1x_2x_3]$$
$$-\left(\frac{2\eta}{1+\zeta}\right)f_{1234}[x_3x_4 + \mathrm{sgn}(\gamma_{\mathbf{G}})x_1x_2] \tag{A6}$$

with

$$f_{1234} = \frac{1}{2}[\gamma_2(1-3) + \gamma_2(1-4) + \gamma_2(2-3) + \gamma_2(2-4) - \gamma_2(1) - \gamma_2(2) - \gamma_2(3) - \gamma_2(4)]. \tag{A7}$$

APPENDIX B: GREEN'S FUNCTION AND MAGNON SELF-ENERGY FOR THE AF PHASE

The time-ordered magnon Green's functions are defined as

$$G_{\alpha\alpha}(\mathbf{k},t) = -i\langle T[\alpha_{\mathbf{k}}(t)\alpha^{\dagger}_{\mathbf{k}}(0)]\rangle, \quad G_{\beta\beta}(\mathbf{k},t) = -i\langle T[\beta^{\dagger}_{-\mathbf{k}}(t)\beta_{-\mathbf{k}}(0)]\rangle,$$

$$G_{\alpha\beta}(\mathbf{k},t) = -i\langle T[\alpha_{\mathbf{k}}(t)\beta_{-\mathbf{k}}(0)]\rangle, \quad G_{\beta\alpha}(\mathbf{k},t) = -i\langle T[\beta^{\dagger}_{-\mathbf{k}}(t)\alpha^{\dagger}_{\mathbf{k}}(0)]\rangle,$$

Considering H_0 as the unperturbed Hamiltonian the Fourier transformed unperturbed propagators are given as

$$G^0_{\alpha\alpha}(\mathbf{k},\omega) = [\omega - E_k + i\delta]^{-1}, \quad G^0_{\beta\beta}(\mathbf{k},\omega) = [-\omega - E_k + i\delta]^{-1}, \tag{B1}$$

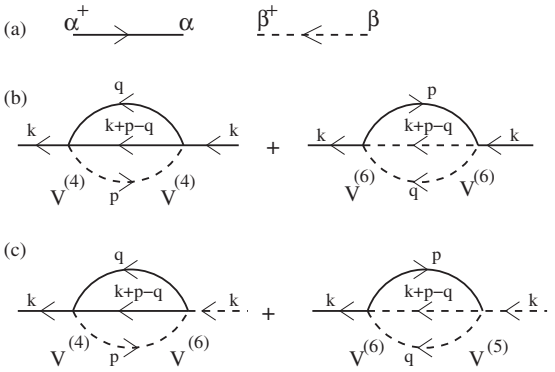

FIG. 16. (a) The solid and the dashed lines correspond to the α and β propagators. Second-order diagrams for the self-energies $\Sigma_{\alpha\alpha}(\mathbf{k},\omega)$ and $\Sigma_{\alpha\beta}(\mathbf{k},\omega)$ are shown in (b) and (c). $V^{(4)}, V^{(5)}, V^{(6)}$ are the vertex factors (see text).

$$G^0_{\alpha\beta}(\mathbf{k},\omega) = G^0_{\beta\alpha}(\mathbf{k},\omega) = 0 \tag{B2}$$

with $\delta \to 0+$. The magnon energy $E_{\mathbf{k}} = \kappa_{\mathbf{k}}\epsilon_{\mathbf{k}}$ is measured in units of $J_1 Sz(1+\zeta)$. The graphical representation of the Green's functions are shown in Fig. 16(a). The full propagators $G_{ij}(\mathbf{k},\omega)$ satisfy the matrix Dyson equation

$$G_{ij}(\mathbf{k},\omega) = G^0_{ij}(\mathbf{k},\omega) + \sum_{mn} G^0_{im}(\mathbf{k},\omega)\Sigma_{mn}(\mathbf{k},\omega)G_{nj}(\mathbf{k},\omega), \tag{B3}$$

where the self-energy Σ_{ij} [$\mathbf{k}$ can be expressed in powers of $1/(2S)$] as

$$\Sigma_{ij}(\mathbf{k},\omega) = \frac{1}{(2S)}\Sigma^{(1)}_{ij}(\mathbf{k},\omega) + \frac{1}{(2S)^2}\Sigma^{(2)}_{ij}(\mathbf{k},\omega) + \cdots. \tag{B4}$$

Using the relations

$$V^{(5)}_{[\mathbf{k+p-q}],\mathbf{q},\mathbf{p},\mathbf{k}} = \mathrm{sgn}(\gamma_{\mathbf{G}})V^{(4)}_{\mathbf{k},\mathbf{p},\mathbf{q},[\mathbf{k+p-q}]},$$

$$V^{(6)}_{\mathbf{q},[\mathbf{k+p-q}],\mathbf{k},\mathbf{p}} = \mathrm{sgn}(\gamma_{\mathbf{G}})V^{(6)}_{\mathbf{k},\mathbf{p},\mathbf{q},[\mathbf{k+p-q}]}$$

the first and second-order self-energies are written as

$$\Sigma^{(1)}_{\alpha\alpha}(\mathbf{k},\omega) = \Sigma^{(1)}_{\beta\beta}(\mathbf{k},\omega) = A_{\mathbf{k}}, \tag{B5}$$

$$\Sigma^{(1)}_{\alpha\beta}(\mathbf{k},\omega) = \Sigma^{(1)}_{\beta\alpha}(\mathbf{k},\omega) = B_{\mathbf{k}}, \tag{B6}$$

$$\Sigma^{(2)}_{\alpha\alpha}(\mathbf{k},\omega) = \Sigma^{(2)}_{\beta\beta}(-\mathbf{k},-\omega) = C_{1\mathbf{k}} + \left(\frac{2}{N}\right)^2 \sum_{\mathbf{pq}} 2l^2_{\mathbf{k}}l^2_{\mathbf{p}}l^2_{\mathbf{q}}l^2_{\mathbf{k+p-q}} \times \left[\frac{|V^{(4)}_{\mathbf{k},\mathbf{p},\mathbf{q},[\mathbf{k+p-q}]}|^2}{\omega - E_{\mathbf{p}} - E_{\mathbf{q}} - E_{\mathbf{k+p-q}} + i\delta} - \frac{|V^{(6)}_{\mathbf{k},\mathbf{p},\mathbf{q},[\mathbf{k+p-q}]}|^2}{\omega + E_{\mathbf{p}} + E_{\mathbf{q}} + E_{\mathbf{k+p-q}} - i\delta}\right], \tag{B7}$$

$$\Sigma^{(2)}_{\alpha\beta}(\mathbf{k},\omega) = \Sigma^{(2)}_{\beta\alpha}(-\mathbf{k},-\omega) = C_{2\mathbf{k}} + \left(\frac{2}{N}\right)^2 \sum_{\mathbf{pq}} 2l^2_{\mathbf{k}}l^2_{\mathbf{p}}l^2_{\mathbf{q}}l^2_{\mathbf{k+p-q}}\,\mathrm{sgn}(\gamma_{\mathbf{G}}) \times V^{(4)}_{\mathbf{k},\mathbf{p},\mathbf{q},[\mathbf{k+p-q}]}V^{(6)}_{\mathbf{k},\mathbf{p},\mathbf{q},[\mathbf{k+p-q}]}\frac{2(E_{\mathbf{p}} + E_{\mathbf{q}} + E_{\mathbf{k+p-q}})}{\omega^2 - (E_{\mathbf{p}} + E_{\mathbf{q}} + E_{\mathbf{k+p-q}})^2}, \tag{B8}$$

where $[\mathbf{k+p-q}]$ is mapped to $(\mathbf{k+p-q})$ in the first BZ by the reciprocal vector $\mathbf{G}$. Feynman diagrams for the second-order self energies are shown in Fig. 16(b) and 16(c). Above the coefficients $C_{1\mathbf{k}}$ and $C_{2\mathbf{k}}$ are

$$C_{1\mathbf{k}} = \frac{1}{2}l^2_k\left(\frac{2}{N}\right)^2 \sum_{12} l^2_1 l^2_2[-6\gamma_1(2-1-\mathbf{k})x_{\mathbf{k}}x_1x_2 + \gamma_1(2)x^2_1x_2 + \gamma_1(2)x^2_{\mathbf{k}}x^2_1x_2 + 2\gamma_1(\mathbf{k})x_{\mathbf{k}}x^2_1 + \gamma_1(1)x^2_{\mathbf{k}}x_1 + \gamma_1(2)x_2]$$
$$- \frac{1}{4}\left(\frac{2\eta}{1+\zeta}\right)l^2_{\mathbf{k}}(1+x^2_{\mathbf{k}})\tilde{C}_{\mathbf{k}}, \tag{B9}$$

$$C_{2\mathbf{k}} = \frac{1}{2}l^2_k\left(\frac{2}{N}\right)^2 \sum_{12} l^2_1 l^2_2[3\gamma_1(2-1-\mathbf{k})x_1x_2 + 3\gamma_1(2-1-\mathbf{k})x^2_{\mathbf{k}}x_1x_2 - 2\gamma_1(1)x_{\mathbf{k}}x_1x^2_2 - 2\gamma_1(2)x_{\mathbf{k}}x_2 - \gamma_1(\mathbf{k})x^2_2 - \gamma_1(\mathbf{k})x^2_{\mathbf{k}}x^2_2]$$
$$- \frac{1}{2}\left(\frac{2\eta}{1+\zeta}\right)l_{\mathbf{k}}m_{\mathbf{k}}\tilde{C}_{\mathbf{k}} \tag{B10}$$

with

$$\tilde{C}_{\mathbf{k}} = \left(\frac{2}{N}\right)^2 \sum_{12} l^2_1 l^2_2\{[2\gamma_2(\mathbf{k}) + \gamma_2(1) + \gamma_2(2) - 4\gamma_2(\mathbf{k}+1-2)]x^2_1 + [\gamma_2(2) - \gamma_2(1+2-\mathbf{k})](1+x^2_1x^2_2)\}. \tag{B11}$$

The divergent terms in $C_{1\mathbf{k}}$ and $C_{2\mathbf{k}}$ for $\mathbf{k} \to 0$ are canceled out by the second terms in Eqs. (B7) and (B8).[13]

APPENDIX C: SECOND-ORDER COEFFICIENTS AND VERTEX FACTORS FOR THE CAF PHASE

The coefficients that appear in the second-order corrections in the Hamiltonian for the CAF phase are

$$C'_{1\mathbf{k}} = \frac{1}{2} l'^2_k \left(\frac{2}{N}\right)^2 \sum_{12} l'^2_1 l'^2_2 [-6\gamma'_1(2-1-\mathbf{k}) x'_{\mathbf{k}} x'_1 x'_2 + \gamma'_1(2) x'^2_1 x'_2 + \gamma'_1(2) x'^2_{\mathbf{k}} x'^2_1 x'^2_2 + 2\gamma'_1(\mathbf{k}) x'_{\mathbf{k}} x'^2_1 + \gamma'_1(1) x'^2_{\mathbf{k}} x'_1 + \gamma'_1(2) x'^2_2]$$
$$- \frac{1}{4}\left(\frac{\zeta}{1+2\eta}\right) l'^2_{\mathbf{k}} (1 + x'^2_{\mathbf{k}}) \tilde{C}'_{\mathbf{k}}, \tag{C1}$$

$$C'_{2\mathbf{k}} = \frac{1}{2} l'^2_k \left(\frac{2}{N}\right)^2 \sum_{12} l'^2_1 l'^2_2 [3\gamma'_1(2-1-\mathbf{k}) x'_1 x'_2 + 3\gamma'_1(2-1-\mathbf{k}) x'^2_{\mathbf{k}} x'_1 x'_2 - 2\gamma'_1(1) x'_{\mathbf{k}} x'_1 x'^2_2 - 2\gamma'_1(2) x'_{\mathbf{k}} x'_2 - \gamma'_1(\mathbf{k}) x'^2_2 - \gamma'_1(\mathbf{k}) x'^2_{\mathbf{k}} x'^2_2]$$
$$- \frac{1}{2}\left(\frac{\zeta}{1+2\eta}\right) l_{\mathbf{k}} m_{\mathbf{k}} \tilde{C}'_{\mathbf{k}}, \tag{C2}$$

where

$$l'_{\mathbf{k}} = \left[\frac{1+\epsilon'_{\mathbf{k}}}{2\epsilon'_{\mathbf{k}}}\right]^{1/2}, \quad m'_{\mathbf{k}} = -\operatorname{sgn}(\gamma'_{\mathbf{k}}) \left[\frac{1-\epsilon'_{\mathbf{k}}}{2\epsilon'_{\mathbf{k}}}\right]^{1/2} = -x'_{\mathbf{k}} l'_{\mathbf{k}} \tag{C3}$$

and

$$\tilde{C}'_{\mathbf{k}} = \left(\frac{2}{N}\right)^2 \sum_{12} l'^2_1 l'^2_2 \{[2\gamma'_2(\mathbf{k}) + \gamma'_2(1) + \gamma'_2(2) - 4\gamma'_2(\mathbf{k}+1-2)] x'^2_1 + [\gamma'_2(2) - \gamma'_2(1+2-\mathbf{k})](1 + x'^2_1 x'^2_2)\}. \tag{C4}$$

For the magnetization and spin-wave dispersion calculations only the vertex factors $V'^{(4)}$ and $V'^{(6)}$ are required which are

$$V'^{(4)}_{1234} = -\gamma'_1(2-4) x'_4 - \gamma'_1(1-4) x'_1 x'_2 x'_4 - \gamma'_1(2-3) x'_3 - \gamma'_1(1-3) x'_1 x'_2 x'_3$$
$$+ \frac{1}{2}[\gamma'_1(2) + \gamma'_1(1) x'_1 x'_2 + \gamma'_1(3) x'_2 x'_3 + \gamma'_1(4) x'_2 x'_4$$
$$+ \gamma'_1(2-3-4) x'_3 x'_4 + \gamma'_1(1-3-4) x'_1 x'_2 x'_3 x'_4 + \gamma'_1(3-2-1) x'_1 x'_3 + \gamma'_1(4-2-1) x'_1 x'_4]$$
$$+ \left(\frac{\zeta}{1+2\eta}\right) f'_{1234} [x'_2 + \operatorname{sgn}(\gamma'_{\mathbf{G}}) x'_1 x'_3 x'_4], \tag{C5}$$

$$V'^{(6)}_{1234} = \gamma'_1(2-4) x'_2 x'_3 + \gamma'_1(2-3) x'_2 x'_4 + \gamma'_1(1-3) x'_1 x'_4 + \gamma'_1(1-4) x'_1 x'_3$$
$$- \frac{1}{2}[\gamma'_1(2) x'_2 x'_3 x'_4 + \gamma'_1(3) x'_4 + \gamma'_1(2-3-4) x'_2 + \gamma'_1(3-2-1) x'_1 x'_2 x'_4$$
$$+ \gamma'_1(1) x'_1 x'_3 x'_4 + \gamma'_1(4) x'_3 + \gamma'_1(1-3-4) x'_1 + \gamma'_1(4-2-1) x'_1 x'_2 x'_3]$$
$$- \left(\frac{\zeta}{1+2\eta}\right) f'_{1234} [x'_3 x'_4 + \operatorname{sgn}(\gamma'_{\mathbf{G}}) x'_1 x'_2] \tag{C6}$$

with

$$f'_{1234} = \frac{1}{2}[\gamma'_2(1-3) + \gamma'_2(1-4) + \gamma'_2(2-3) + \gamma'_2(2-4) - \gamma'_2(1) - \gamma'_2(2) - \gamma'_2(3) - \gamma'_2(4)]. \tag{C7}$$

*majumdak@gvsu.edu

[1] H. M. Rønnow, D. F. McMorrow, R. Coldea, A. Harrison, I. D. Youngson, T. G. Perring, G. Aeppli, O. Syljuasen, K. Lefmann, and C. Rischel, Phys. Rev. Lett. **87**, 037202 (2001).

[2] N. B. Christensen, D. F. McMorrow, H. M. Ronnow, A. Harrison, T. G. Perring, and R. Coldea, J. Magn. Magn. Mater. **272-276**, 896 (2004).

[3] N. B. Christensen, H. M. Ronnow, D. F. McMorrow, A. Harrison, T. G. Perring, M. Enderle, R. Coldea, L. P. Regnault, and G. Aeppli, Proc. Natl. Acad. Sci. U.S.A. **104**, 15264 (2007).

[4] A. Bombardi, J. Rodriguez-Carvajal, S. Di Matteo, F. de Bergevin, L. Paolasini, P. Carretta, P. Millet, and R. Caciuffo, Phys. Rev. Lett. **93**, 027202 (2004).

[5] R. Melzi, P. Carretta, A. Lascialfari, M. Mambrini, M. Troyer, P. Millet, and F. Mila, Phys. Rev. Lett. **85**, 1318 (2000).

[6] R. Melzi, S. Aldrovandi, F. Tedoldi, P. Carretta, P. Millet, and F. Mila, Phys. Rev. B **64**, 024409 (2001).

[7] P. Carretta, N. Papinutto, C. B. Azzoni, M. C. Mozzati, E. Pavarini, S. Gonthier, and P. Millet, Phys. Rev. B **66**, 094420 (2002).

[8] Y. J. Kim *et al.*, Phys. Rev. Lett. **83**, 852 (1999).
[9] R. Coldea, S. M. Hayden, G. Aeppli, T. G. Perring, C. D. Frost, T. E. Mason, S.-W. Cheong, and Z. Fisk, Phys. Rev. Lett. **86**, 5377 (2001).
[10] H. W. de Wijn, R. E. Walstedt, L. R. Walker, and H. J. Guggenheim, Phys. Rev. Lett. **24**, 832 (1970).
[11] R. E. Walstedt, H. W. de Wijn, and H. J. Guggenheim, Phys. Rev. Lett. **25**, 1119 (1970).
[12] E. Pavarini, S. C. Tarantino, T. B. Ballaran, M. Zema, P. Ghigna, and P. Carretta, Phys. Rev. B **77**, 014425 (2008).
[13] J. I. Igarashi, Phys. Rev. B **46**, 10763 (1992).
[14] J. I. Igarashi, J. Phys. Soc. Jpn. **62**, 4449 (1993).
[15] J. I. Igarashi and T. Nagao, Phys. Rev. B **72**, 014403 (2005).
[16] L. Capriotti, Int. J. Mod. Phys. B **17**, 4819 (2003).
[17] G. E. Castilla and S. Chakravarty, Phys. Rev. B **43**, 13687 (1991).
[18] A. B. Harris, D. Kumar, B. I. Halperin, and P. C. Hohenberg, Phys. Rev. B **3**, 961 (1971).
[19] P. Chandra and B. Doucot, Phys. Rev. B **38**, 9335 (1988).
[20] S. Chakravarty, B. I. Halperin, and D. R. Nelson, Phys. Rev. B **39**, 2344 (1989).
[21] C. M. Canali and S. M. Girvin, Phys. Rev. B **45**, 7127 (1992).
[22] C. M. Canali, S. M. Girvin, and M. Wallin, Phys. Rev. B **45**, 10131 (1992).
[23] A. V. Syromyatnikov, J. Phys.: Condens. Matter **22**, 216003 (2010).
[24] T. Roscilde, A. Feiguin, A. L. Chernyshev, S. Liu, and S. Haas, Phys. Rev. Lett. **93**, 017203 (2004).
[25] A. V. Dotsenko and O. P. Sushkov, Phys. Rev. B **50**, 13821 (1994).
[26] N. Shannon, B. Schmidt, K. Penc, and P. Thalmeier, Eur. Phys. J. B **38**, 599 (2004).
[27] L. Isaev, G. Ortiz, and J. Dukelsky, Phys. Rev. B **79**, 024409 (2009).
[28] O. A. Starykh and L. Balents, Phys. Rev. Lett. **93**, 127202 (2004).
[29] V. N. Kotov, J. Oitmaa, O. P. Sushkov, and Z. Weihong, Phys. Rev. B **60**, 14613 (1999).
[30] V. N. Kotov and O. P. Sushkov, Phys. Rev. B **61**, 11820 (2000).
[31] A. A. Nersesyan and A. M. Tsvelik, Phys. Rev. B **67**, 024422 (2003).
[32] B. Schmidt, M. Siahatgar, and P. Thalmeier, Phys. Rev. B **81**, 165101 (2010).
[33] Zheng Weihong, J. Oitmaa, and C. J. Hamer, Phys. Rev. B **43**, 8321 (1991).
[34] C. J. Hamer, Zheng Weihong, and P. Arndt, Phys. Rev. B **46**, 6276 (1992).
[35] Zheng Weihong, J. Oitmaa, and C. J. Hamer, Phys. Rev. B **44**, 11869 (1991).
[36] Zheng Weihong and C. J. Hamer, Phys. Rev. B **47**, 7961 (1993).
[37] J. Oitmaa and Zheng Weihong, Phys. Rev. B **54**, 3022 (1996).
[38] Weihong Zheng, J. Oitmaa, and C. J. Hamer, Phys. Rev. B **71**, 184440 (2005).
[39] P. Sindzingre, Phys. Rev. B **69**, 094418 (2004).
[40] X. Wang, Mod. Phys. Lett. B **14**, 32 (2000).
[41] T. Hakobyan, J. H. Hetherington, and M. Roger, Phys. Rev. B **63**, 144433 (2001).
[42] S. R. White and A. L. Chernyshev, Phys. Rev. Lett. **99**, 127004 (2007).
[43] J. R. Viana and J. R. de Sousa, Phys. Rev. B **75**, 052403 (2007).
[44] G. Mendonca, R. Lapa, J. R. de Sousa, M. A. Neto, K. Majumdar and T. Datta, J. Stat. Mech.: Theor. Exp. (2010) P06022.
[45] R. F. Bishop, P. H. Y. Li, R. Darradi, and J. Richter, J. Phys.: Condens. Matter **20**, 255251 (2008).
[46] A. A. Tsirlin and H. Rosner, Phys. Rev. B **79**, 214417 (2009).
[47] A. W. Sandvik and R. R. P. Singh, Phys. Rev. Lett. **86**, 528 (2001).
[48] L. Capriotti, F. Becca, A. Parola, and S. Sorella, Phys. Rev. B **67**, 212402 (2003).
[49] S. Yunoki and S. Sorella, Phys. Rev. Lett. **92**, 157003 (2004).
[50] H. T. Diep, *Frustrated Spin Systems*, 1st ed. (World Scientific, Singapore, 2004).
[51] S. Sachdev, *Quantum Phase Transitions*, 1st ed. (Cambridge University Press, Cambridge, UK, 2001).
[52] R. R. P. Singh, Z. Weihong, C. J. Hamer, and J. Oitmaa, Phys. Rev. B **60**, 7278 (1999).
[53] O. P. Sushkov, J. Oitmaa, and Weihong Zheng, Phys. Rev. B **63**, 104420 (2001).
[54] O. Volkova *et al.*, Phys. Rev. B **82**, 054413 (2010).
[55] O. Janson, A. Tsirlin, and H. Rosner, arXiv:1007.2798 (unpublished).
[56] G. H. Liu, H. L. Wang, and G. S. Tian, Phys. Rev. B **77**, 214418 (2008).
[57] T. Hikihara and O. A. Starykh, Phys. Rev. B **81**, 064432 (2010).
[58] H. H. Hung, C.-D. Gong, Y.-C. Chen, and M.-F. Yang, Phys. Rev. B **73**, 224433 (2006).
[59] E. H. Kim, O. Legeza, and J. Solyom, Phys. Rev. B **77**, 205121 (2008).
[60] T. Holstein and H. Primakoff, Phys. Rev. **58**, 1098 (1940).
[61] T. Oguchi, H. Nishimori, and Y. Taguchi, J. Phys. Soc. Jpn. **54**, 4494 (1985).
[62] N. B. Christensen (private communication).
[63] A. V. Syromyatnikov (private communication).
[64] M. Roger, J. Phys. Chem. Solids **66**, 1412 (2005).
[65] K. P. Schmidt and G. S. Uhrig, Mod. Phys. Lett. B **19**, 1179 (2005).
[66] D. A. Huse, Phys. Rev. B **37**, 2380 (1988).